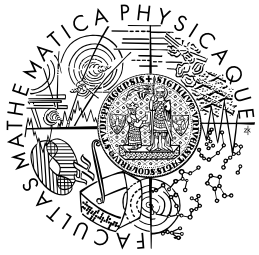

FACULTY
OF MATHEMATICS
AND PHYSICS
Charles University

BACHELOR THESIS

Terézia Košíková

Hydrosphere structure of icy satellites

Department of Geophysics

Supervisor of the bachelor thesis: doc. RNDr. Marie Běhounková, Ph.D.

Study programme: Physics (B0533A110001)

Study branch: FP (0533RA110001)

Prague 2023

I declare that I carried out this bachelor thesis independently, and only with the cited sources, literature and other professional sources. It has not been used to obtain another or the same degree.

I understand that my work relates to the rights and obligations under the Act No. 121/2000 Sb., the Copyright Act, as amended, in particular the fact that the Charles University has the right to conclude a license agreement on the use of this work as a school work pursuant to Section 60 subsection 1 of the Copyright Act.

In ..... date ....

Author's signature

I would like to thank doc. RNDr. Marie Běhounková, Ph.D. for her help, patience and willingness to supervise my bachelor thesis. I would also like to thank my family and friends for their moral support, not only during the writing of my bachelor thesis but throughout my whole studies.

Title: Hydrosphere structure of icy satellites

Author: Terézia Košíková

Department: Department of Geophysics

Supervisor: doc. RNDr. Marie Běhounková, Ph.D.

Abstract: The exploration of potential life on other celestial bodies within the Solar System is one of the key questions in planetary science. In this work, we focused on determining the hydrosphere of the icy moons Ganymede and Europa in order to determine possible obstacles in habitability due to the presence of the high-pressure ices. We used known thermodynamic properties and satellite parameters to create an algorithm that determined their structures. We found that on Ganymede high-pressure ices are present in a wide range of pressure and temperature conditions, which may prevent the transfer of minerals between the silicates and the subsurface ocean. For Europa, we found that the occurrence of high-pressure ice phases is very unlikely in its hydrosphere. However, the latest data for Europa complicates the exact determination of its structure and Europa may contain thinner hydrosphere and ocean than originally thought.

Keywords: icy satellites, ice, thermodynamic properties, structure

Název práce: Struktura hydrosféry ledových měsíců

Autor: Terézia Košíková

Katedra: Katedra geofyziky

Vedoucí bakalářské práce: doc. RNDr. Marie Běhounková, Ph.D.

Abstrakt: Skúmanie potenciálneho života na iných nebeských telesách v rámci Slnečnej Sústavy je jednou z kľúčových otázok planetárnej vedy. V tejto práci sme sa zamerali na určenie hydrosféry ľadových mesiacov Ganymede a Europa, aby sme určili možné prekážky v obývateľnosti v dôsledku prítomnosti vysokotlakových fázy ľadu. Použili sme známe termodynamické vlastnosti a parametre satelitov na vytvorenie algoritmu, ktorý určil ich štruktúru. Zistili sme, že na Ganymede sú vysokotlakové ľady prítomné v širokom rozsahu tlakových a teplotných podmienok, ktoré môžu brániť prenosu minerálov medzi silikátmi a podpovrchovým oceánom. Pre Európu sme zistili, že výskyt vysokotlakových ľadových fázy je v jej hydrosfére veľmi nepravdepodobný. Najnovšie údaje pre Európu však komplikujú presné určenie jej štruktúry a Európa môže obsahovať tenšiu hydrosféru a oceán, ako sa pôvodne predpokladalo.

Klíčová slova: ľadové satelity, ľad, termodynamické vlastnosti, štruktúra

Contents

1. Introduction

The investigation of habitability beyond the Earth serves as a driving force for the exploration of planetary bodies within our Solar System. Among the biggest candidates for extraterrestrial life in the Solar System (e.g., Taubner et al., 2020) are the moons of the giant planets (see Fig. 1.1). Jupiter's Galilean moons Europa, Ganymede, and Callisto are notable candidates with a large habitable potential. Similarly, Saturn's moons Titan and Enceladus have been discussed in this context. In the last few years, the possible existence of life even on the moons of Uranus and Neptune has been discussed (Bierson and Nimmo, 2022; Castillo-Rogez et al., 2023). One of the main criteria, by which candidates for the existence of life are determined, is the assumption of the existence of a subsurface ocean in their structure.

The existence of a global inner ocean in large icy moons (Ganymede, Europa, Callisto) was suspected since the early 1970s (Lewis, 1971). The extent of the ocean depends on many factors, such as thermal state, ocean and hydrosphere composition, as well as satellites' material properties. Voyager 1, Voyager 2, the Galileo mission, the Cassini mission and the New Horizon mission improved our knowledge of the internal structure of these satellites, however in the case of Uranus and Neptune's satellites only in a limited amount.

The water-rock interaction plays an essential role as a component in the origin of life, during which important, necessary minerals are released (e.g., Vance et al., 2016). Within larger icy moons, such as Ganymede, Titan and Callisto, however, these interactions may be impeded or even completely prevented due to the presence of high-pressure (HP) ice layers, i.e., HP ice phases, which arise due to high pressures inside the satellites.

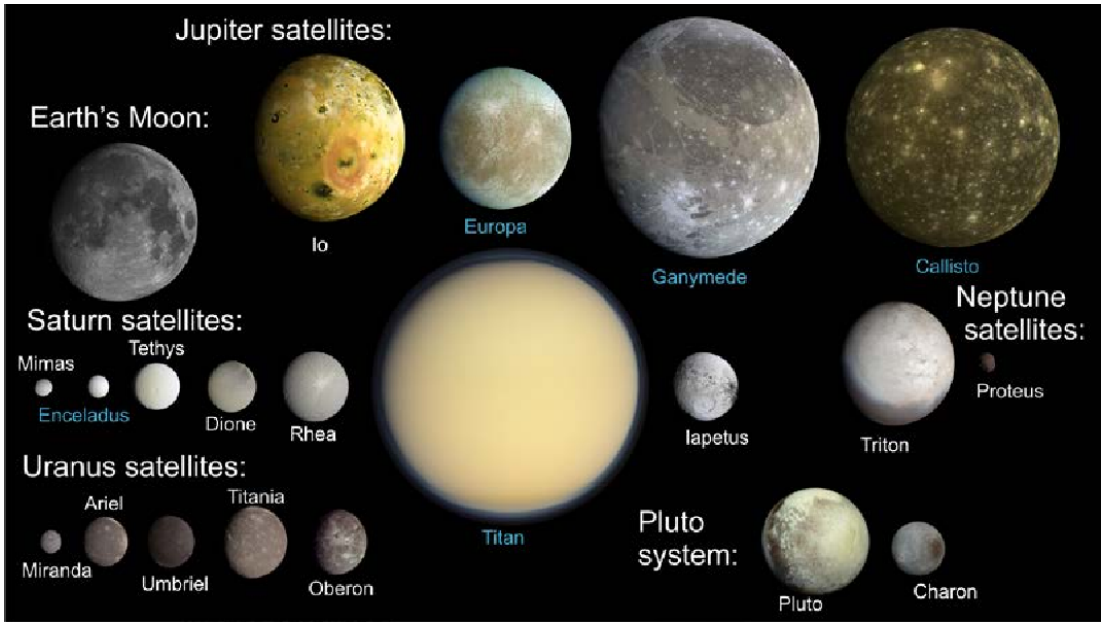

Figure 1.1: Satellites of outer Solar System compared to Earth's Moon. Adapted from Nimmo (2018).

These layers would be located between the liquid layer and the silicates, thus preventing their direct contact with each other. However, if the HP ice layer were to melt, it may allow direct or indirect water-rock interaction (Kalousová et al., 2018).

In this thesis, we will concentrate on the hydrosphere structure, its extent, and the possible existence of HP ices. In the first chapter, we will introduce the basic knowledge and equations for the interior structure of bodies in general, and we will take a closer look at the two icy moons of Jupiter: Ganymede and Europa. In the second chapter, we will approach thermodynamic theory and equations used in our calculations, such as phase transitions of ice, Gibbs free energy, and other thermodynamic variables necessary for determining the structure of satellites. The third chapter will present the algorithm, used in our code, with the help of which we determined the structure of the icy moons. In the last chapter, we apply our code, and we summarize and discuss the specific results of the calculations for Ganymede and Europa.

2. Interior structure of icy satellites

Due to a lack of direct data, understanding and modelling the interior structure of icy satellites can be challenging. The main characteristics used for assessing interior structures are mass and radius, shape, gravity and magnetic fields, observed activity on the surface, surface temperatures and heat flow and composition of the surface and atmosphere of the specific satellite. In our work, we will mainly focus on the gravity field, mass and radius of the satellites.

2.1 Planetary radius, mass and moment of inertia factor

For many bodies, the average radius R and shape of the satellite can be observed directly, whether from ground-based telescopes or images produced by close-by flying spacecraft. Close flybys of spacecrafts, as well as the interaction of the satellite with other bodies, can determine multipole expansion of the gravitational field. The information about the gravitational field is, however, limited for icy satellites; only moments for degrees $l = 0$ and $l = 2$ are usually available. Degree $l = 0$ provides information about the mass of the planet M

$$g = \frac{GM}{r^2}, \tag{2.1}$$

where G represents the Newtonian constant of gravitation, $r > R$ is the radius, g is the gravitational acceleration at r. Assuming hydrostatic equilibrium, the gravitational coefficients on degree $l = 2$, allows us to assess the polar moment of inertia C. Both the mass M and polar moment of inertia C provide essential information on the internal structure and density distribution.

Usually, when modelling the interior structure, the polar moment of inertia C is translated into a moment of inertia factor (MoI). It's a dimensionless characteristic sensitive to radial mass distribution inside the satellite. The lower the MoI value, the more is mass concentrated towards the centre of the satellite. Values of MoI for many icy satellites are determined. All the acceptable models of the density profile inside the interior structures must match these values. MoI can be obtained from the polar moment of inertia C, mass M and surface radius R:

$$\text{MoI} = \frac{C}{MR^2}. \tag{2.2}$$

With the help of the material properties, we use these observations to assess the internal structure of satellites. Assuming a spherically symmetric body, or body in hydrostatic equilibrium, the total mass of a satellite can be derived from equation (Vance et al., 2014):

$$M = 4\pi \int_0^R \rho(r) r^2 dr, \tag{2.3}$$

where $\rho(r)$ is the density, dependent on the radial distance from the satellite's interior.

Polar moment of inertia C is calculated as (Hussmann et al., 2010):

$$C = \frac{8\pi}{3} \int_0^R \rho(r) r^4 dr, \tag{2.4}$$

where $\rho(r)$ is the density, dependent on the radial distance from the satellite's interior.

2.2 Icy satellites

We chose Ganymede and Europa as representative moons for assessing the structure because they both represent different types of icy moons (Fig. 2.1). Ganymede is the largest moon in the Solar System. It is certainly differentiated and the presence of high-pressure ice phases in its hydrosphere is very likely.
On the contrary, the exact structure for Europe is not certain from the latest measurements. Its hydrosphere is probably small, and the presence of a high-pressure ice phase is very unlikely.

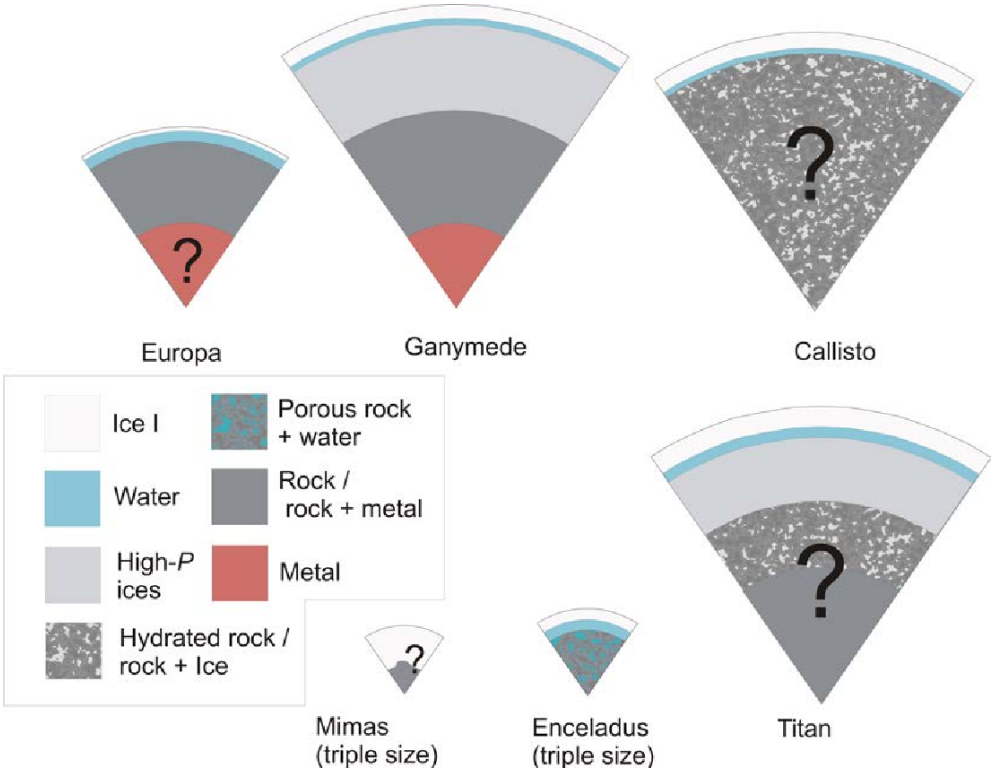

Figure 2.1: Internal structure for few satellites. Our interest lies in the structure of Europa and Ganymede. Adapted from Nimmo (2018).

2.2.1 Ganymede

Ganymede is one of the four Galilean moons, orbiting Jupiter, with a radius of 2634 km, and a mean density of 1940 kg/m^3 (Lissauer and Pater, 2013). It is the largest satellite in our Solar System. Assuming hydrostatic equilibrium, with gravity data from Ganymede provided by the Galileo mission, Ganymede's moment of inertia factor (MoI), which characterizes the radial distribution of mass inside the satellite, was calculated. With a value of 0.3115 ± 0.0028 (Schubert et al., 2004), Ganymede has the lowest MoI value among solid satellites, and also terrestrial planets, in our Solar System.

Ganymede's size and low MoI, however, are not the only thing distinguishing it from other satellites. As Galileo's magnetometer discovered, Ganymede has its own internal magnetic field, strong enough to form its own mini-magnetosphere inside the magnetosphere of Jupiter. The most reasonable interpretation of its existence is a magnetic dynamo located in Ganymede's liquid metallic core, most likely a Fe-FeS core (Schubert et al., 1996). However, a dipole magnetic field of Ganymede cannot fully explain the magnetic data obtained by Galileo's mission. In order to explain the remaining signal, Kivelson et al. (2002) proposed two models. A model representing the internal field as the sum of dipole and quadrupole terms of the magnetic field, and a model presenting the magnetic field as an induced magnetic dipole in conducting layer. The latter model places a conductive layer at a depth of 170 km to 460 km, therefore suggesting that Ganymede may have a subsurface salty liquid layer in its hydrosphere. Kivelson et al. (2002) states that both models fit the data, but prefers the induced magnetic field model, due to the less amount of parameters needed to describe the internal sources of magnetic fields (the quadrupole model requires 8, while the induced magnetic field model only 4).

Small values of MoI for Ganymede and the existence of its internally generated magnetic field suggest enough heating for differentiation of liquid, metallic, iron-rich core and silicate mantle (Journaux et al., 2020b). The model used for describing Ganymede's internal structure is a three-layer model, which best suffices the gravity, density and magnetic field data (Lissauer and Pater, 2013). The innermost layer is constructed of a liquid metallic core surrounded by a silicate mantle layer, where each layer is predicted to be around 900 km thick. Above these layers is then located a thick H_2O layer, or in other words, hydrosphere. The thickness of Ganymede's hydrosphere is assumed to exceed 800km. Because of high-pressure values at the bottom of the hydrosphere, the existence of HP ice layers is inevitable below a depth of around 150km (Hussmann et al., 2010). The temperature in this depth corresponds to the minimal melting temperature of H_2O. Data states, Ganymede's hydrosphere was subdivided into layers of Ih-ice, III-ice, V-ice and VI-ice (Hussmann et al., 2010). The hypothetical layer of liquid H_2O would be located between Ih-ice and III-ice, V-ice and VI-ice layer, which would prevent significant water-rock interactions. However, if heat transfer is efficient enough, high-pressure ice layers could be melted, enabling therefore, a direct water-rock interface. The efficiency of the transfer is determined by the thermodynamic and rheological properties.

The liquid layer does not need to consist only of pure H_2O, however. In general, it has been broadly assumed, that the ocean composition of icy satellites consists of H_2O-$MgSO_4$ solution (Vance et al., 2014).

2.2.2 Europa

With respect to distance from Jupiter, Europa is the second of the Galilean moons, with a radius of 1560 km. Its mean density is 3018 kg/m^3, placing it between those of icy satellites, such as Ganymede or Callisto, and rock satellites such as Io or Earth's Moon (Hussmann et al., 2010). The value of Europa's mean density indicates a rock/ice composition, where the rock layer provides more than 90% of the mass, meaning less than 10% of mass is contributed by the hydrosphere. The top of the hydrosphere is covered by solid water ice. The proof was provided by Voyager and Galileo imaging and infrared spectroscopy (Sohl et al., 2002). The thickness of the ice layer is uncertain (Howell, 2021). It can be only a few kilometres or tens of kilometres. The existence of a subsurface liquid H_2O ocean in Europa's hydrosphere is indirectly proven by the satellite's surface topology, but mainly by measurements of Jupiter's magnetic field near Europa (Khurana et al., 1998).

Comparing Ganymede and Europa, it is obvious Europa is a significantly smaller satellite with a higher value of mean density. This indicates that Europa has a higher representation of silicates than Ganymede, and therefore smaller hydrosphere. The pressures inside it will not reach such high values as in large icy satellites, therefore the presence of high-pressure ice phases in its hydrosphere is very unlikely. The liquid layer, therefore, lays directly between the ice shell and rock interior, meaning interactions at the water-rock interface are present.

As in the case of Ganymede, thanks to data from close flybys of the Galileo mission, the MoI for Europa was determined, the value of which is 0.3405 ± 0.0022 (Jacobson et al., 2000). This value leans towards a model, where Europa's interior is fully differentiated into metal core, silicate mantle and H_2O layer, as is the case of Ganymede. The size of the core in this model corresponds to roughly half of the total radius of the satellite (Sohl et al., 2002). However, more recent additional data from the Juno mission offered a new value for MoI that was significantly larger than the previous one, 0.3547 ± 0.0024 (Gomez Casajus et al., 2021). This new value may question the assumption on the three-layer model for Europe and may suggest the use of a two-layer model, consisting of a H_2O layer and a silicate core. The chemical composition introduces yet another complexity if carbon-rich icy satellites are considered (Reynard and Sotin, 2023).

3. Thermodynamic properties

Understanding the thermodynamic properties of ice (Fig. 3.1), particularly its high-pressure phases plays a vital role in gaining insights into the structure of the hydrosphere. To date, experimental studies have confirmed the existence of twenty distinct crystalline polymorphs of ice (Komatsu, 2022), and the number is still growing. Moreover, about three orders of magnitude more are assumed via calculations (Engel et al., 2018).

The pressure-temperature (PT) conditions ranging from 0.1 to 2000 MPa, below room temperature, are of particular interest when studying icy satellites. Under these PT conditions, most polymorphs (i.e., Ih, *Ic, II, III, *IV, V, VI, *IX, XI, *XII, *XIII, *XIV and XV; metastable phases marked with an asterisk) was found. While exploring the icy moons, the attention is focused mainly on stable ice phases Ih, II, III, V, VI (Journaux et al., 2020b).

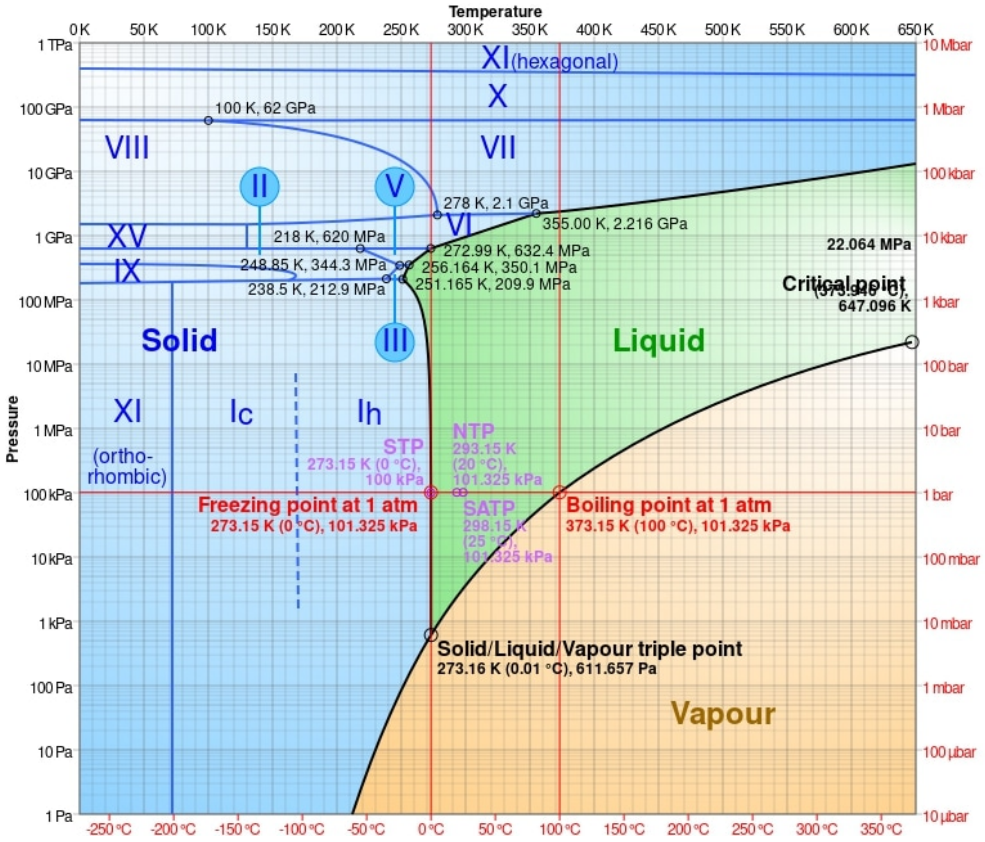

Figure 3.1: Phase diagram of water with temperature up to 650 K and pressure from 1 Pa to 1 TPa. Adapted from Wikipedia (2023).

3.1 Gibbs free energy

Ices thermodynamics and the ice/water phase diagram are commonly represented through Gibbs free energy G, a thermodynamic potential depending on pressure P and temperature T. Gibbs free energy is classically used for equilibrium calculations in chemical reactions and phase transitions. Furthermore, all equilibrium thermodynamic properties, including specific volume, specific heat, and thermal expansivity, can be derived from analytical derivatives of the Gibbs free energy for a system in thermodynamic equilibrium (Journaux et al., 2020a).

Gibbs free energy, as a function of pressure and temperature, can be calculated from equation (Journaux et al., 2020a):

$$G(P,T) = \int_{P_0}^{P} V(P',T)dP' + G(P_0,T), \tag{3.1}$$

where $G(P_0,T)$ it the temperature-dependent Gibbs free energy at ambient pressure and $V(P,T)$ is the specific volume. Temperature dependence of $G(P_0,T)$ can be parameterized by:

$$G(P_0,T) = G_0(P_0,T_0) - S_0(P_0,T_0)(T-T_0) + \int_{T_0}^{T} C_P(T')dT' - T\int_{T_0}^{T} \frac{C_P(T')}{T'}dT', \tag{3.2}$$

where $G_0(P_0,T_0)$ is the reference Gibbs free energy and S_0 is the reference entropy, usually representing values at the temperature of absolute zero and ambient pressure or some specific thermodynamic invariant, such as triple point. C_P represents the specific heat for constant pressure. For calculating specific volume in Equation (3.1), Journaux et al. (2020a) suggest using Mie-Grüneisen equation of state, which gives values of specific volume for a wide range of temperature and pressure values.

The chemical potential μ is frequently used as an alternative to Gibbs free energy. The relationship between Gibbs free energy and chemical potential is straightforward: the chemical potential of a substance represents the Gibbs free energy per mole. In other words, the molar Gibbs free energy is equal to the chemical potential (Callen, 1985).

Here, we will use two different parameterizations of the thermodynamic properties (Journaux et al., 2020a; Choukroun and Grasset, 2010) and their implementations.

3.2 SeaFreeze

The first method we used for determining thermodynamic properties is the SeaFreeze library (Journaux et al., 2020a; Bollengier et al., 2019). SeaFreeze is an open-source library hosted on GitHub. Its purpose is to calculate the thermodynamic (and elastic) properties of water and ice polymorphs Ih, II, III, V, VI for temperatures in the range 220 - 500K and pressures from 0 - 2300 MPa, using Gibbs parametrization given in Equation (3.1).

The library is readily available for use and contains the most recent data, with continuous updates being added. However, alongside its advantages, it also possesses certain limitations. The first drawback is the computational time required for calculations. In comparison to the second method (Section 3.3), the

calculations are several times slower. The second limitation is that the provided relationships in the library only apply to liquid layers with zero salinity, in contrast to the work by Vance et al. (2014), where salinity values ranging from 0 to 10 wt% are considered. However, as part of the planned updates for SeaFreeze, information will be incorporated into the usage of aqueous solutions, specifically for solutions containing NaCl, $MgSO_4$, and NH_3.

3.3 PhaseDiag

Pure water

The second approach in this study is based on the works of Choukroun and Grasset (2007), Choukroun and Grasset (2010), Vance and Brown (2013) and Vance et al. (2014) for the composition of pure water. It uses the chemical potential μ to determine the stable phase (μ minimization), through Equations (3.1) and (3.2) rewritten per mole.

Choukroun and Grasset (2010) used a set of equations and parameters that allowed calculating all the values for all the polymorphs with a single formulation using chemical potential μ. Moreover, they describe chemical potentials of phases $\mu^S_{\mathrm{H_2O}}$ relatively to the liquid chemical potential $\mu^L_{\mathrm{H_2O}}$ phase

$$\Delta\mu_{\mathrm{H_{20}}} = \mu^S_{\mathrm{H_2O}}(P,T) - \mu^L_{\mathrm{H_2O}}(P,T). \tag{3.3}$$

In this formulation, the reference term in Equations (3.1) and (3.2) are expressed as the enthalpy difference

$$\Delta H_0 = T_0 \Delta S_0, \tag{3.4}$$

where T_0 is a reference condition of temperature; ΔS_0, defined as a difference of entropy of solid and liquid phase. The values for reference pressure P_0, reference temperature T_0 and reference entropy variation of liquid and solid phase ΔS_0 are stated in Choukroun and Grasset (2010).

For our calculation, heat capacities are temperature-dependent. Choukroun and Grasset (2010) suggests using for heat capacities at constant pressure C_p of solid ice phases:

$$C_p^S(T) = c_0 + c_1 T + \frac{c_2}{T^2}, \tag{3.5}$$

Coefficients c_0, c_1 and c_2 are constants. Their values are listed in Choukroun and Grasset (2010).

Calculating heat capacities for the liquid phase is more complicated. Definitions are divided by temperature: below the temperature of 231 K is used a 7^{th} degree polynomial approximation, and over 231 K an exponential approximation.

$$T \leq 231K : C_p^L(T) = \sum_{n=0}^{7} c_i T^i, \tag{3.6}$$

$$T \geq 231K : C_p^L(T) = c_0 + c_1 \exp(c_2(T - T_{ref})). \tag{3.7}$$

Coefficients c_i of 7^{th} polynomial approximation, coefficient c_0,c_1,c_2 of exponential approximation and reference temperature T_{ref} are constants.

Their values together with the coefficients for the solid phases are listed (Choukroun and Grasset, 2010).

For specific volume, Choukroun and Grasset (2010) derived a new formulation, which is accurate, effective and easily used:

$$V(P,T) = V_0\zeta_1(T)\zeta_2(P), \tag{3.8}$$

where V_0 represents an arbitrary volume of reference, and ζ_1 and ζ_2 are functions describing relations of specific volume on temperature and pressure.

$$\zeta_1(T) = 1 + a_0 \tanh(a_1(T - T_{ref})), \tag{3.9}$$
$$\zeta_2(P) = b_0 + b_1(1 - \tanh(b_2 P)). \tag{3.10}$$

Coefficients a_0 ,a_1 ,b_0 ,b_1 ,b_2 and T_{ref} are again constant. Values of coefficients a_0 ,a_1 ,b_0 ,b_1 ,b_2 and T_{ref} for liquid and each ice polymorphs used in equations are listed in Choukroun and Grasset (2010).

Thermodynamic theory for $H_2O-MgSO_4$ solution

The aforementioned approaches do not consider the influence of salt or any anti-freezing agents on phase stability. In the presence of a specific salt concentration, phase equilibrium occurs at the PT point, where the chemical potential of the solid phase (S) is equal to that of the liquid phase (L): $\mu^S = \mu^L$. Using the general formulation for a non-ideal solution, the chemical potential of aqueous $MgSO_4$ can be expressed as (Vance et al., 2014):

$$\mu^L_{\mathrm{H_2O}}(P,T,X^L_{\mathrm{H_2O}}) = \mu^L_{\mathrm{H_2O}}(P,T,1) + RT\ln\Big(\gamma^L_{\mathrm{H_2O}}X^L_{\mathrm{H_2O}}\Big), \tag{3.11}$$

where $X^L_{\mathrm{H_2O}}$ is the mole (or molar) fraction of liquid water; $\gamma^L_{\mathrm{H_2O}}$ is the activity coefficient of liquid water, which can be defined as:

$$RT\ln\Big(\gamma^L_{\mathrm{H_2O}}\Big) = W(1 - X^L_{\mathrm{H_2O}})^2. \tag{3.12}$$

Coefficient W, called the Margules coefficient, is expressed as:

$$W = w_0(1 + w_1\tanh(w_2 P))(1 + w_3/(T - T_0)^2), \tag{3.13}$$

where $w_{i=1,2,3}$ and T_0 are constant and they are stated in Vance et al. (2014).

To describe the thermodynamic properties of the $MgSO_4$ solution as function of pressure P, temperature T and concentration C ($\alpha(P,T,C)$, $C_p(P,T,C)$, $\rho(P,T,C)$), we use the tables in Vance and Brown (2013) and the linear interpolation contained in the Scipy library in Python.

Implementation

All the above equations, together with the coefficients and with the equation for $\Delta\mu_{\mathrm{H_2O}}$, and with the preparation for drawing the corresponding phase diagrams, were taken from a library PhaseDiag (Košíková, 2022) created for SFG. The validity of parameterization is up to 2.2 GPa for pure water and ice (Choukroun and Grasset, 2010). The properties (ρ, C_p, α) of aqueous $MgSO_4$

is valid up to 800 MPa at temperatures $250 - 370$ K. In our calculations for Ganymede, however, it was necessary to find a corresponding pressure value of up to 1.5 GPa. For higher pressure, we can afford the extrapolation for salinity values up to 10wt% because in this case, it is smooth in all thermodynamic properties.

Remarks on concentration

Using Equation (3.11) can be determined chemical potential μ, taking into account the effect of the salt concentration in the ocean. In the calculations, the value of wt% could not be used directly. It had to be converted to a molar fraction X. Here, we state their mutual relations used in this work.

The salinity value is given in wt%, the percentage of the mass fraction w_i (McNaught and Wilkinson, 1997).

$$w_i = \frac{m_i}{m_{tot}}, \tag{3.14}$$

$$\sum_{i=1}^{n} w_i = 1, \tag{3.15}$$

where m_i equals mass of the substance ($MgSO_4$), and m_{tot} represents total mass of the mixture. Limited by the fact that at salinity values higher than 10wt%, the occurrence of high-pressure ices is small, we chose to work with values 0wt%, 3wt%, 5wt% and 10wt% in our model.

A mole fraction is defined as a unit of the amount of a component, divided by the total amount of all components in a mixture (McNaught and Wilkinson, 1997).

For two-component solution, the conversion of wt%, or more precisely, mass fraction w to the mole fraction X is mediated by the formula:

$$X_A = \frac{M_B w_A}{w_A(M_B - M_A) + M_A}, \tag{3.16}$$

where w_A is the mass fraction, M_A is the molar mass of the substance, which w_A is known, and M_B is the molar mass of the remaining substance in the mixture.

However, when we calculated the adiabatic gradient in the ocean Equation (4.10), or the values of ρ, c_p, and α in the ocean, molality was used instead of the mole fraction X. Molality, or molal concentration, is defined as the amount of substance of solute (in moles), divided by the mass of the solvent (McNaught and Wilkinson, 1997). The conversion of mole fraction X to molality b is mediated by the formula:

$$b_A = \frac{X_A}{M_A(1 - X_A)}. \tag{3.17}$$

3.4 Phase diagrams

As described in Sections 3.2 and 3.3, to calculate thermodynamic parameters, and thus to draw phase diagrams, we used two approaches. In the figures Fig. 3.2(a) and Fig. 3.2(b), the diagram is plotted using the method described in Section 3.3, for an ocean salt concentration of 0wt% and 10wt%. Figure Fig. 3.2(c) shows the phase diagram for zero salt concentration using the method described in Section 3.2.

Comparing Fig. 3.2(a) and Fig. 3.2(c) we see that the phase diagrams differ slightly. Figure Fig. 3.2(c) also includes II-ice, which is turned off in Fig. 3.2(a). However, as will be shown in Chapter 5, II-ice does not even appear in our results, so this difference is not significant for our purposes. In addition to the phase II difference, the diagrams also differ in the size of phase III and V, but this difference is not drastic and is probably due to SeaFreeze working with more recent data and different parameterization.

a) PhaseDiag- 0wt%

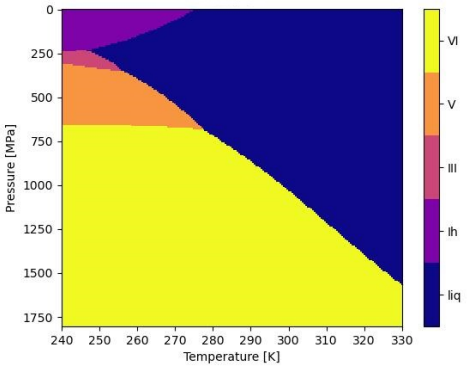

b) PhaseDiag- 10wt%

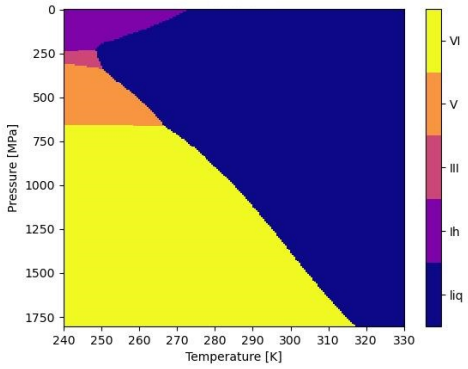

c) SeaFreeze- 0wt%

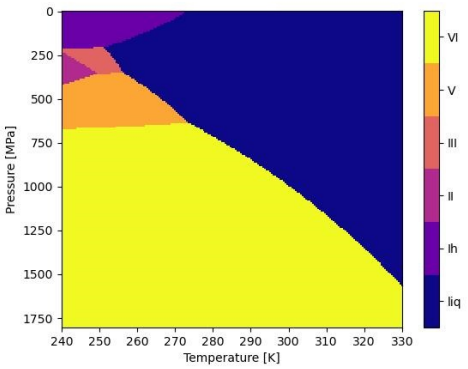

Figure 3.2: Phase diagrams, using method PhaseDiag for 0wt% and 10wt%, and SeaFreeze for 0wt%. Note different colour schemes for PhaseDiag and SeaFreeze.

4. Interior model

Our objective was to develop a model of the hydrospheres of icy moons by utilizing information about their size, mass, and moment of inertia factor, along with experimental data on water/ice properties. To describe the interior of the satellite's deeper layers (the silicate mantle and iron-rich core), we employ simplified properties characterized by their respective constant densities (see Section 4.1).

In the case of the hydrospheres, we consider the thermodynamic properties of water and ices, which may also contain dissolved $MgSO_4$ as discussed in the previous chapter. These properties are dependent on both pressure P and temperature T. As a first step, we need to determine the temperature and pressure profiles as functions of depth (see Sections 4.2 and 4.3). Subsequently, we outline the iterative procedure employed to obtain the structure of the hydrosphere (see Section 4.4).

4.1 Two-layer and three-layer models of interior structure

When discussing models of interior structures of icy satellites, two simplified layered models are considered. A two-layer model, consisting of a silicate-metal core and H_2O layer, and a three-layer model, consisting of metal core, silicate mantle and H_2O layer. Note that the hydrosphere (H_2O layer) is divided into sublayers with varying densities and properties. The core and mantle are simplified and we assume to have a constant density.

Two-layer models, consisting of the hydrosphere and silicate-metal core, may be reasonable to use with medium-sized ice satellites of Jupiter, Saturn, and Uranuswhen the conditions are not favourable for full differentiation. For larger icy satellites, assuming they are fully differentiated, the two-layer model is not sufficient anymore. In the case of Ganymede, it possesses the internally generated magnetic field (Kivelson et al., 2002), which can be generated in a fluid iron core. For a description of its internal structure is used three-layer model, consisting of the hydrosphere, rock mantle and metal core.

For the N-layer model ($N \geq 2$), the value of MoI can also be used to describe the internal structure, provided that the value is determined from close spacecraft flybys, using the expression for the mass Equation (2.3) and moment of inertia Equation (2.4).
We are generally interested in values for the hydrosphere, so we can split M and C into contributions from the hydrosphere and the solid interior of satellites. For the three-layer model, the equations for the calculation are (Vance et al., 2014):

$$M = M_{\mathrm{H_2O}} + \frac{4\pi}{3}[\rho_{mantle}(R_{mantle} - R_{core})^3 + \rho_{core}R_{core}^3], \tag{4.1}$$

$$M_{\mathrm{H_2O}} = 4\pi \int_{R_{sil}}^{R} \rho(r) r^2 dr, \tag{4.2}$$

$$C = C_{\mathrm{H_2O}} + \frac{8\pi}{15}[\rho_{mantle}(R_{mantle} - R_{core})^5 + \rho_{core}R_{core}^5], \tag{4.3}$$

$$C_{\mathrm{H_2O}} = \frac{8\pi}{3} \int_{R_{sil}}^{R} \rho(r) r^4 dr, \tag{4.4}$$

where $M_{\mathrm{H_2O}}$ denotes the total mass of the hydrosphere, $C_{\mathrm{H_2O}}$ the moment of inertia of the hydrosphere, R_{mantle} represents the mantle radius, ρ_{mantle} the density of the mantle, R_{core} the core radius and ρ_{core} the density of a core. For the two-layer model, we simply use limit $R_{core} \to 0$.

To solve the contribution of core and mantle to the total mass and MoI (Equations 4.1 and 4.3) and thus calculate M and C for the three-layer model, we need to know densities and radii for core and mantle, i.e. four independent variables. However, only two conditions are known (mass M and MoI). Consequently, two of the parameters need to be prescribed, so the remaining can be calculated. We choose to prescribe densities, as suggested in Vance et al. (2014). For the two-layer model, only mantle radius and density needed to be determined, and they are computed from the knowledge of the total mass of the body M and the polar moment of inertia C.

4.2 Temperature profile

In order to be able to calculate the temperature T at a given depth, it is necessary to introduce several assumptions. Following Vance et al. (2014), we consider the conductive heat transfer in the Ih-ice layer, the adiabatic temperature profile in the liquid ocean, and the temperature profile following the liquidus line to approximate two-phase flow in high-pressure ices.

The steady-state conductive heat transfer with no internal heating is described as follows

$$\nabla \cdot k \nabla T = 0, \tag{4.5}$$

where T is the temperature, k is the conductivity. We assume temperature-dependent conductivity:

$$k = \frac{D}{T}, \tag{4.6}$$

where parameter D is equal to $632\,\mathrm{W\,m^{-1}}$ (Andersson and Inaba, 2005). We assume that the Ih-ice layer is thin ($d \ll R$) and we can solve the above equation in the Cartesian domain and that the solution is independent of the horizontal coordinates ($\frac{\partial T}{\partial x} = \frac{\partial T}{\partial y} = 0$). Under the above conditions, Equation (4.5) can be rewritten as

$$\begin{aligned} \frac{\partial}{\partial z}\left(\frac{D}{T(z)}\frac{\partial}{\partial z}T(z)\right) &= 0, \\ T(z) &= A\exp\left\{\frac{Bz}{D}\right\}, \end{aligned} \tag{4.7}$$

where z is the depth, and A and B are the constants of integration, determined using the boundary conditions.

We solve the above equation for the fixed bottom (at the Ih ice-water interface, $T(z_b) = T_b$) and surface temperature $T(z = 0) = T_0$. We vary bottom temperature T_b between 250 K and 270 K because it corresponds to the liquidus

with ice Ih over the range of eutectic temperatures for the aqueous $MgSO_4$ sulfate system (Vance et al., 2014). The surface temperature T_0 complies with the observations. The solution of Equation (4.7) reads:

$$T(z) = T_b^{z/z_b} T_0^{1-z/z_b}. \tag{4.8}$$

Specifically, in our calculations, we chose the values T_b = 255, 260, 265 and 270K from this interval. Corresponding heat flux at the Ih-ice and liquid interface q_b is calculated using the formula:

$$q_b = D\frac{\ln T_b/T_0}{z_b}. \tag{4.9}$$

In the liquid ocean layer, an adiabatic profile is assumed, described by the equation:

$$\frac{\mathrm{d}T}{\mathrm{d}P} = \frac{\alpha T}{\rho C_p}, \tag{4.10}$$

where α is the volumetric thermal expansion, ρ is the density and C_p is the heat capacity at constant pressure.

In high-pressure ices (HP ices), the temperature follows the liquidus line to approximate two-phase flow (Šrámek et al., 2007).

4.3 Pressure profile

By knowing the density, denoted as $\rho(P, T, C)$, we can calculate the pressure and gravitational acceleration profiles. It is important to note that the gravitational acceleration in the hydrosphere is not constant. As we move deeper into the ice and liquid layers and approach the mantle and core, gravitational acceleration increases due to the significantly higher densities of the deep layers. This means that the values in the hydrosphere can differ by up to 25% from the surface value of gravitational acceleration, denoted as g_{surf}.

To calculate pressure P for a given radius, as well as gravitational acceleration g at a given radius, we use the following differential equations, assuming a spherically symmetric body (Valencia et al., 2006):

$$\frac{\mathrm{d}g}{\mathrm{d}r} = 4\pi G\rho(r) - \frac{2Gm(r)}{r^3}, \tag{4.11}$$

$$\frac{\mathrm{d}P}{\mathrm{d}r} = -\rho(r)g(r), \tag{4.12}$$

where G is the gravitational constant, r represent the radius, $m(r)$ mass in the underlying layers, derived from Equation (4.2), and $\rho(r)$ is density at given depth.

4.4 Algorithm for assessing the structure

Besides the thermodynamic properties of ice/water, the planetary body is described by its surface radius R, mass M, and moment of inertia factor MoI. We also assume temperature at the Ih ice-ocean boundary T_b and the salinity of the ocean $wt\%$. The surface temperature was assumed as the average surface

temperature of Ganymede (Weissman et al., 2007). The polar moment of inertia C was calculated from the value of MoI and Equation (2.2). The gravitational acceleration at the surface g_{surf} was derived from Equation (2.1).

In the case of the three-layer material model, we fix the density of the mantle ρ_{mantle} and the core ρ_{core}. The radius of the mantle R_{mantle} and the core R_{core} is determined from the knowledge of the mass and MoI. For the two-layer material model, the average density of the mantle ρ_{mantle} and the mantle radius R_{mantle} is assessed from the mass and MoI.

We compute the internal structure iteratively. During each iteration j, we utilize the explicit one-step method with constant integration step to integrate from the surface to the interior. In each iteration, we assume that we know the depth of the Ih ice-ocean interface z_b from the previous iteration. The procedure ends when $\left|\frac{z_b^j - z_b^{j-1}}{z_b^{j-1}}\right| < \varepsilon = 10^{-8}$. Less than ten iterations are needed to reach this convergence criterion.

For the first iteration step $j = 1$, we estimate the thickness of the Ih-ice layer using a simple equation:

$$z_b^{j=1} = \frac{p_b}{g_{surf}\rho_{iceIh_{ref}}}, \tag{4.13}$$

where g_{surf} is the gravitational acceleration on the surface, $\rho_{iceIh_{ref}}$ represents the reference value of density for Ih-ice; P_b represents pressure at the Ih ice-ocean interface at temperature T_b and it is found from Ih-ice liquidus curve. The reference values used in our computations are written in tables Tab. 5.1 for Ganymede and Tab. 5.16 for Europa.

For each iteration j, the body was split into two sections: Ih-layer and the rest of the body and each section was further divided into layers. The i-th layer is represented by a value of the radius r_i, and we integrate along the radius r.

Specifically, the Ih-ice layer was divided into N_1 equidistant layers. New values of temperature $T_i(r)$ via conductive temperature profile (Equation 4.8), pressure $P_i(r)$ (Equation 4.12), gravitational acceleration $g_i(r)$ (Equation 4.11) were determined at i-th integration step. The density value $\rho_i(P_i, T_i)$ was computed using values established in the previous step. The specific procedures for calculating the given thermodynamic parameters were described in Chapter 3.

The rest of the body was divided into N_2 steps. The same variables as in the Ih-ice layer were determined using the same approach, apart from computing T_i. The algorithm always tests which phase is stable. If the liquid water phase was stable, the adiabatic profile of temperature (Equation 4.10) was used for computing T_i; the density $\rho(P_i, T_i, w)$ of the ocean also depends on the salinity. If the HP-ice phase was stable, T_i was computed by following the liquidus line.

Along with thermodynamic properties, new values of the mass of the hydrosphere $M^i_{\mathrm{H_2O}}$ and the moment of inertia of the hydrosphere $C^i_{\mathrm{H_2O}}$ were calculated using Equations (4.2) and (4.4). The radius of mantle R^i_{mantle} was determined as the radius at the following integration step r_i. For the three-layer model, the radius of a core R^i_{core} was calculated from the mass of the body M Vance et al. (2014):

$$R^i_{core} = \left(\frac{M - M^i_{\mathrm{H_2O}} - \frac{4\pi}{3}\rho_{mantle}\left(R^i_{mantle}\right)^3}{\frac{4\pi}{3}(\rho_{core} - \rho_{mantle})} \right)^{1/3}, \tag{4.14}$$

where M is the total mass of the moon and $M_{\mathrm{H_2O}}$ is the mass of the hydrosphere in

the corresponding depth. Similarly, the density of the mantle ρ_{mantle} is determined from the total mass of the body M

$$\rho_{mantle} = \frac{M}{\frac{4}{3}\pi R^3_{mantle}}. \tag{4.15}$$

Using the overall moment of inertia of a hydrosphere in Equation (4.3), we also analytically determine the value of the total moment of inertia of the satellite. This value at i-th integration step served as a control point $C^i_{control}$. For the i-th integration step, $C^i_{control}$ was calculated and compared with the observed moment of inertia of the satellite C. The radial integration stops once $C^i_{control}$ reaches the desired value C.

Last but not least, we determined the thickness of each layer of the hydrosphere once the converged solution is found. The method used for that was dependent on a stable phase at each depth. The stable phase needed to be established from the chemical potential, resp. Gibbs free energy, as the minimal value for the corresponding PT conditions.

The implementation of the algorithm was part of this work, it is available on GitLab (Košíková, 2023), and it was compared with Vance et al. (2014). The convergence for increasing N_1 and N_2 was tested. The differences between the two solutions are small and can be attributed to a slightly different numerical approach.

5. Results

The focus of this chapter is to determine the structure of icy satellites, using the approach and numerical solution introduced in the previous chapter. The structure was determined for two icy moons, namely Ganymede and Europa. For Ganymede, the method PhaseDiag based on (Vance et al., 2014; Choukroun and Grasset, 2010) for four values of salt concentration was used, as well as the method using the SeaFreeze library for zero salt concentration. Europa's structure was determined only using the PhaseDiag method.

As mentioned in the previous chapter, in order to determine the structure of the icy satellite, the following available parameters for respective satellites are used: average planetary radius R, the total mass of the satellite M, and moment of inertia factor MoI or polar moment of inertia C.

We have included two free parameters: the temperature of the ocean at the Ih ice-ocean interface T_b and the concentration of salt in the ocean $wt\%$. Since these parameters are unknown in reality, we will systematically vary them to determine the effect on the structure. Additionally, the structural model of the body was chosen, i.e. whether it was a two- or three-layer model. If the three-layer model was used, it was also necessary to enter the densities for the mantle ρ_{mantle} and core ρ_{core}.

5.1 Ganymede

The structure was determined for Ganymede, using a three-layer model, as the iron-rich core is essential to explain the presence of its magnetic field. Ocean temperatures T_b were successively taken from the interval $\{255, 260, 265, 270\}$ K, for $MgSO_4$ salt concentrations in values of {0,3,5,10} wt%. Physical parameters for Ganymede along with reference values are listed in Tab. 5.1. Values of ρ_{core} and ρ_{mantle} were taken:

$$\rho_{mantle} = 3250\,\mathrm{kg\,m^{-3}},$$
$$\rho_{core} = 7030\,\mathrm{kg\,m^{-3}}.$$

This value ρ_{mantle} represents the average representation of dehydrated silicates in the mantle, while ρ_{core} represents a situation where the Fe-FeS representation ratio in the core is 25% FeS (Vance et al., 2014).

Parameter	Value
T_{surf} [K]	110
M [kg]	$1.48{\cdot}10^{23}$
MoI (Schubert et al., 2004)	0.3115
R [km]	2634.1
C [kg m^2]	$3.20{\cdot}10^{29}$
g_{surf} [m s^{-2}]	1.4
$\rho_{iceI_{ref}}$ [kg m^{-3}]	920

Table 5.1: Reference parameters for Ganymede.

The resulting thicknesses of individual parts of the hydrosphere D_{Ih-ice}, D_{liq}, D_{II-ice}, $D_{III-ice}$, D_{V-ice}, D_{VI-ice}, together with the radii of the silicate mantle R_{mantle}, and metal core R_{core}, and the corresponding value of heat flux q_b are listed in the tables Tab. 5.2 - Tab. 5.5.

The results show that as the ocean temperature T_b increases, the HP-ice layer shrinks, as does the Ih-ice layer. Thus, the ocean thickness in the hydrosphere must increase. The same trend, albeit smaller, also occurs for constant T_b and increasing salt concentrations in the ocean.

As expected, the Ih-ice layer decreases with increasing salt concentration. For HP-ices, however, the situation can be more complex. The III-ice layer does not occur for ocean temperatures T_b equal to or greater than 255 K. We also observe increasing VI-ice layer thickness, due to the decrease of the mantle radius. This is necessary to fit M and MoI due to the increase of the water density and different PT conditions of the phase transitions. Additionally, the V-ice layer is present up to temperatures $T_b = 260$ K, except for the case of 10 wt%, where at this temperature the value equals zero.

Changing T_b, as well as increasing wt%, also affects the size of the mantle and core. For 0wt%, R_{mantle} also increases for increasing T_b (Tab. 5.2). Additionally, in most cases, the value of R_{core} decreases. However, we observe the opposite trend for non-zero values of wt%, due to the anomalous behaviour of water for low salt concentration. For a salt concentration of 0, 3 & 5 wt%, the mutual differences of R_{core} and R_{mantle} for the respective temperatures are relatively moderate. However, for 10 wt%, the values of R_{core} and R_{mantle} differ significantly more than those for the remaining salt concentrations.

By comparing our results presented in Tab. 5.2, Tab. 5.3, Tab. 5.4 and Tab. 5.5 with values listed in Vance et al. (2014), we see the thicknesses for layers differ. One of the reasons why the results slightly differ from those presented in Vance et al. (2014) was the use of different MoI values. Vance et al. (2014) states MoI $= 0.3105 \pm 0.0028$, which does not match the value, written in Tab. 5.1, which we used. The reason we chose a different MoI was that the value we used is the value used as Ganymede's MoI in most sources (Schubert et al., 2004).

To synthesize the results, we present density as a function of pressure for 0 wt% (Fig. 5.1) and 10 wt% (Fig. 5.2) salinity, showing the dependence for temperatures T_b=$\{255, 260, 265, 270\}$ K.

Fig. 5.1 and Fig. 5.2 depict Ganymede's hydrosphere structure with density jumps corresponding to phase transitions. As an example, we will take Fig. 5.1 graph of density dependence on pressure for T_b=255 K. For pressure from 0-200 MPa, we observe a curve that corresponds to the density of the Ih-ice layer. From a pressure of 200 MPa to 400 MPa, we then observe a curve corresponding to density within the ocean determined by pressure and temperature following the adiabatic profile. Subsequently, for higher pressures, we observe densities corresponding to the course of HP-ice, specifically for V-ice and VI-ice in this case.

Fig. 5.3 shows the phase diagram for zero salt concentration for temperatures T_b=$\{255, 260, 265, 270\}$ K and temperature profiles. The phase diagram for a 10 wt% salt concentration for T_b=$\{255, 260, 265, 270\}$ K is shown in Fig. 5.4. The heat flow at the Ih-ice and the liquid interface is equal to the heat that must be produced in the deeper part of the satellites for the given structure to

PhaseDiag - 0wt%	N_1 = **21*50**	N_2= **200*50**		
T_b [K]	255	260	265	270
q_b [mW m^{-2}]	3.85	4.86	6.85	12.65
Ih-ice [km]	137.896	111.961	81.084	44.86
Liquid [km]	110.094	210.115	358.735	478.539
III-ice [km]	0	0	0	0
V-ice [km]	164.017	93.076	0	0
VI-ice [km]	392.692	384.665	353.628	267.495
R_{mantle} [km]	1829.401	1834.283	1840.653	1843.205
R_{core} [km]	623.031	616.013	610.292	614.835

Table 5.2: PhaseDiag - 0wt% : Results for structure of Ganymede.

PhaseDiag - 3wt%	N_1 = **21*50**	N_2= **200*50**		
T_b [K]	255	260	265	270
q_b [mW m^{-2}]	3.96	5.03	7.22	14
Ih-ice [km]	134.251	108.067	76.977	40.527
Liquid [km]	114.005	210.44	357.266	483.75
III-ice [km]	0	0	0	0
V-ice [km]	160.256	91.199	0	0
VI-ice [km]	403.766	402.943	377.213	287.915
R_{mantle} [km]	1821.822	1821.452	1822.644	1821.908
R_{core} [km]	638.233	640.996	645.064	655.258

Table 5.3: PhaseDiag - 3wt% : Results for structure of Ganymede.

PhaseDiag - 5wt%	N_1 = **21*50**	N_2= **200*50**		
T_b [K]	255	260	265	270
q_b [mW m^{-2}]	4.06	5.21	7.58	15.377
Ih-ice [km]	130.741	104.4	73.295	36.906
Liquid [km]	121.175	219.853	365.463	502.867
III-ice [km]	0	0	0	0
V-ice [km]	153.722	81.464	0	0
VI-ice [km]	411.593	415.165	384.671	287.538
R_{mantle} [km]	1816.86	1813.217	1810.67	1806.789
R_{core}	648.083	656.895	666.809	681.387

Table 5.4: PhaseDiag - 5wt% : Results for structure of Ganymede.

PhaseDiag - 10wt%	N_1 = **21*50**	N_2= **200*50**		
T_b [K]	255	260	265	270
q_b [mW m^{-2}]	4.5	5.95	9.13	22.21
Ih-ice [km]	118.006	91.425	60.87	25.55
Liquid [km]	173.376	317.357	458.338	700.205
III-ice [km]	0	0	0	0
V-ice [km]	104.177	0	0	0
VI-ice [km]	438.347	437.892	338.928	153.398
R_{mantle} [km]	1800.194	1787.425	1775.964	1754.947
R_{core} [km]	679.658	703.287	725.975	758.668

Table 5.5: PhaseDiag - 10wt% : Results for structure of Ganymede.

be stable. The sources can be tidal heating (although in the case of Ganymede, this process has only a small contribution), or radioactive decay in the mantle.

We observe that the estimated heat flux increases rapidly with increasing ocean temperature T_b, as well as with increasing wt%, which indicates that with increasing temperature, as well as with increasing salt concentration, a higher amount of heat is needed to maintain the stability of the structure.

Comparing the phase diagram for 0 wt% and 10 wt%, we see that the line representing the HP ice-ocean interface is steeper when the salt concentration in the ocean is higher. We also observe that the course of the temperature profiles corresponds to the resulting thicknesses of the individual layers of the hydrosphere.

In the phase diagrams, we also show the temperature profiles corresponding to the ocean temperatures T_b=$\{255, 260, 265, 270\}$ K. As expected, we observe the conductive heat transfer in the Ih-ice, followed by an adiabatic temperature profile in the liquid layer. When we then encounter HP ices, the temperature profile begins to follow the liquidus line to approximate two-phase flow and temperate ice in high-pressure ices. The temperature profile ends at the point when we hit the mantle of the satellite and thus leave the hydrosphere.

In the next computation, the SeaFreeze library was used. The physical parameters used were the same as in the previous computation, written in Tab. 5.1. The resulting thicknesses are written in Tab. 5.6. Again, graphs of density dependence on pressure (Fig. 5.5) and phase diagrams were plotted, however, SeaFreeze allows us to only compute with salt concentrations 0 wt% (Fig. 5.5).

SeaFreeze - 0 wt% N_1 **= 21*50** N_2**= 200*50**				
T_b [K]	255	260	265	270
q_b [mW m^{-2}]	4.024	5.301	8.053	19.162
Ih-ice [km]	132.041	102.551	69.001	29.615
Liquid [km]	142.381	282.296	378.390	483.441
III-ice [km]	0	0	0	0
V-ice [km]	114.356	9.114	0	0
VI-ice [km]	420.388	407.873	352.480	285.741
R_{mantle} [km]	1824.934	1832.265	1834.229	1835.304
R_{core} [km]	625.717	616.447	619.731	626.424

Table 5.6: SeaFreeze - 0 wt% : Results for structure of Ganymede.

By comparing the results measured using the SeaFreeze library with the results from the previous computation in Tab. 5.2, we notice several differences. The Ih-ice layer measured by SeaFreeze is smaller compared to the previous computation, as is the V-ice layer. On the other hand, the thickness of the liquid layer is greater, as is the VI-ice layer. The radius of mantle R_{mantle} and the radius of core R_{core} are similar in both approaches, only differing in units of kilometres. In the case of T_b=260 K, the values of R_{core} differ only in tenths of a kilometre. We observe a higher heat flux than in the previous computation, especially for higher temperatures T_b.

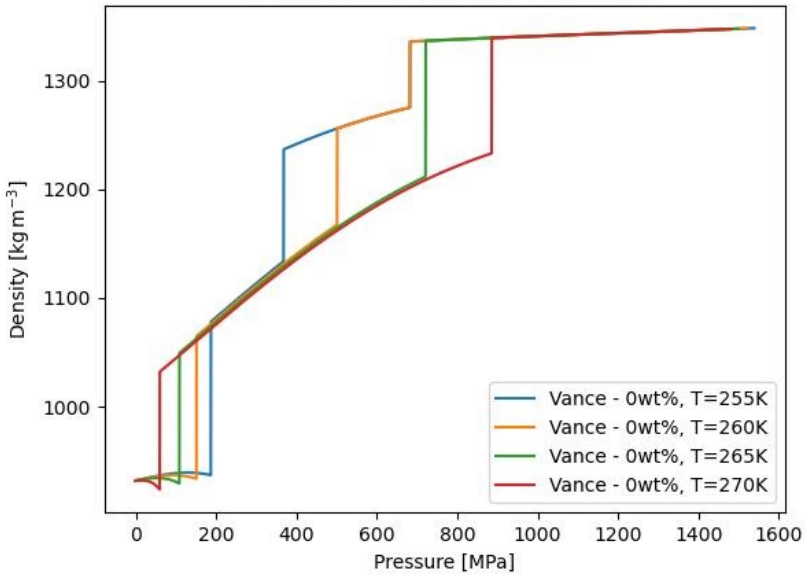

Figure 5.1: Density as a function of pressure for Ganymede with 0 wt% salt concentration in the ocean, using PhaseDiag approach.

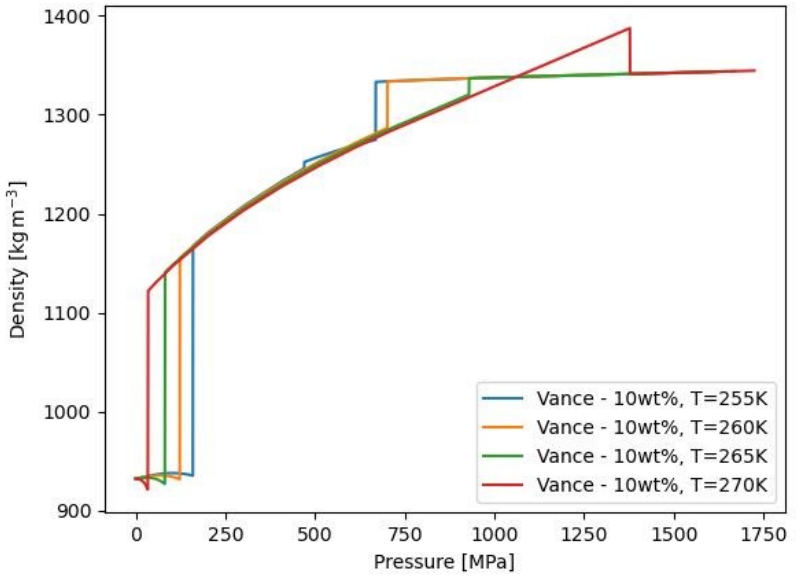

Figure 5.2: Density as a function of pressure for Ganymede with 10 wt% salt concentration in the ocean, using PhaseDiag approach.

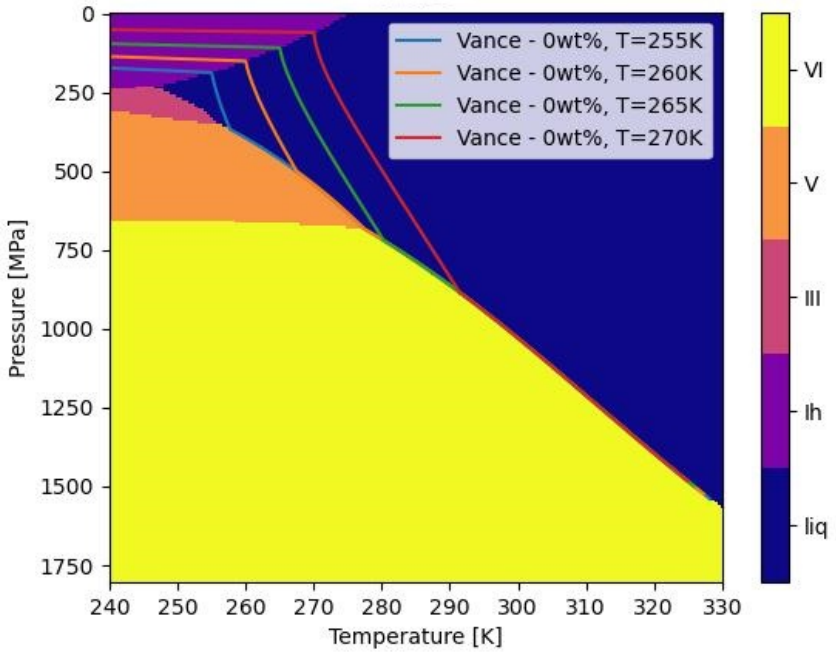

Figure 5.3: Phase diagram and temperature profile for Ganymede with 0 wt% salt concentration in the ocean, using PhaseDiag approach.

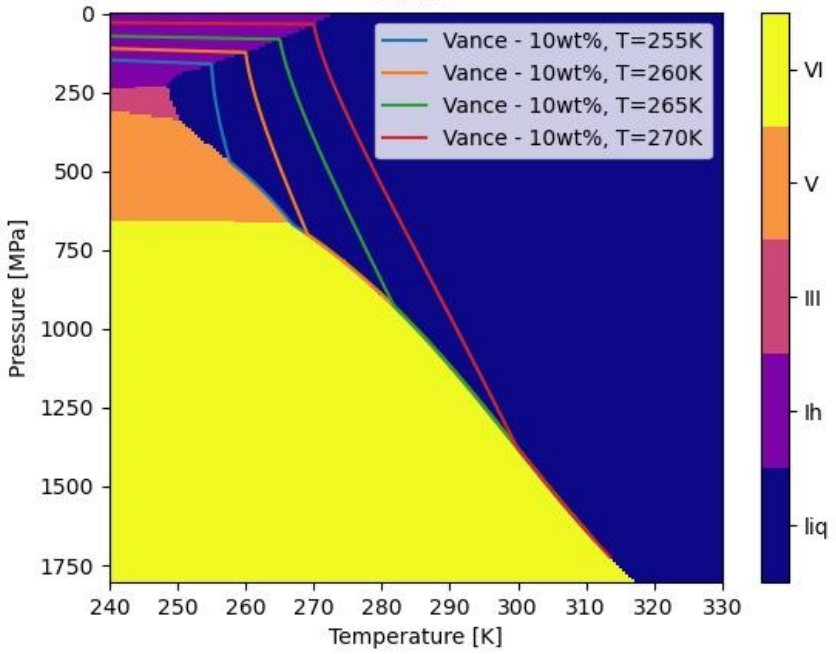

Figure 5.4: Phase diagram and temperature profile for Ganymede with 10 wt% salt concentration in the ocean, using PhaseDiag approach.

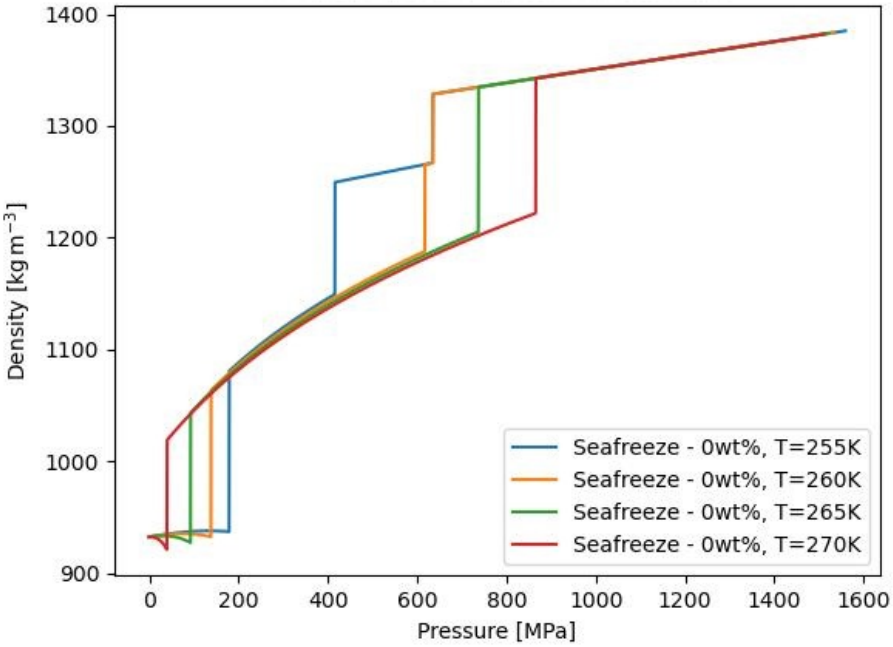

Figure 5.5: Density as a function of pressure for Ganymede with 0 wt% salt concentration in the ocean, using approach from SeaFreeze library.

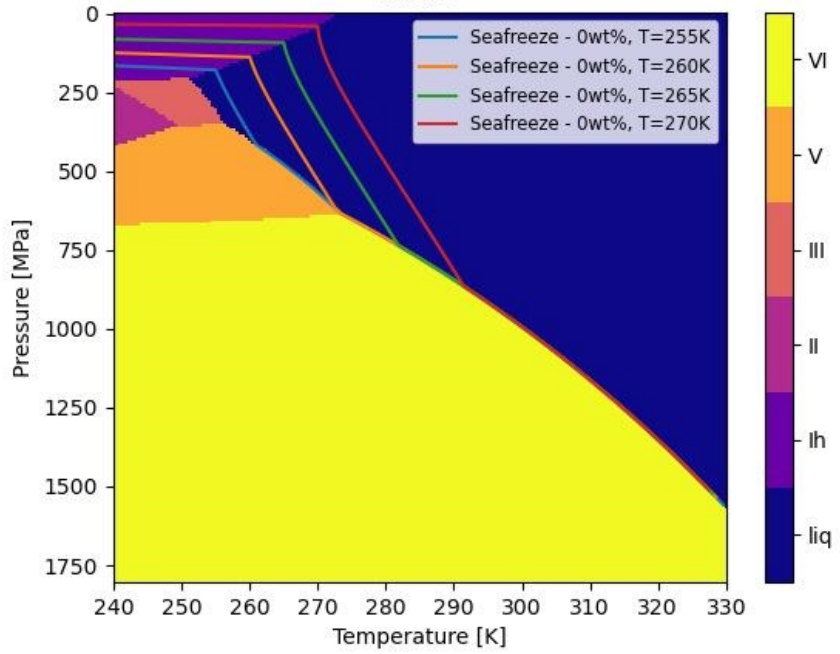

Figure 5.6: Phase diagram and temperature profile for Ganymede with 0 wt% salt concentration in the ocean, using approach from SeaFreeze library.

It is important to note that errors in the structure, and the differences in results between the PhaseDiag and SeaFreeze methods are also due to the use of different thermodynamic descriptions. Therefore, the uncertainties for the thermodynamic properties should be included to assess the errors in the structure determination.

Finally, we focused on the effect of the change in densities for the core ρ_{core} and the mantle ρ_{mantle} on the hydrosphere. Again we used physical parameters taken from Tab. 5.1. The values of ρ_{mantle} were taken from the interval $\{2500, 3250, 3550\}$ kg m^{-3}, where the smallest value corresponds to situations when the silicates formed the mantle are fully hydrated/saturated. The highest value corresponds to the case when the silicate mantle is not hydrated and Fe_2SiO_4 are taken into account. For the core, the density ρ_{core} was taken from the interval $\{5150, 7030, 8000\}$ kg m^{-3}. The eutectic Fe-FeS core is represented by the lowest value, the case when the core is pure iron corresponds to the highest value of the interval. The results are recorded in Tab. 5.7 - Tab. 5.15.

The results showed that the heat flux, as well as almost the entire hydrosphere, does not significantly depend on the density of the core or the density of the mantle. The only component of the hydrosphere that changes is the VI-ice thickness, to fit M and MoI. We observe that, in general, it increases rapidly with increasing ρ_{mantle}, on the contrary, it generally decreases with increasing ρ_{core}. Also, as was observed in other computations, it decreases with increasing value of T_b and increases with increasing concentration of salt in the ocean. Specifically, for $\rho_{mantle} = 2500\,\mathrm{kg\,m^{-3}}$, we observe that with changing ρ_{core} the changes in the thickness of the VI are relatively large. At the density of $\rho_{mantle} = 3250\,\mathrm{kg\,m^{-3}}$, the change associated with the increase in the value of ρ_{core} is almost negligible, only in the order of km. And at $\rho_{mantle}= 3550\,\mathrm{kg\,m^{-3}}$, we observe the changes are almost non-existent, only in order of tenths of kilometres at most in our resolution.

The highest value of the mantle density is obtained from the knowledge presented in Vance et al. (2014), which says that for models where iron cores do not occur in the satellite structure, the mantle density must be higher than $3600\,\mathrm{kg\,m^{-3}}$, which corresponds to our results. Equal and higher values than $3600\,\mathrm{kg\,m^{-3}}$ were tested in the measurement. For these values, we received the radius of the core equal to zero. However, this does not meet the prerequisites, since we know that Ganymede must be fully differentiated, based on the small MoI and the existence of an internal magnetic field (Journaux et al., 2020b).

To synthesize the tabular results, graphs were drawn showing the dependencies of the core radius R_{core} and the mantle radius R_{mantle} on the mantle density ρ_{mantle} at constant values of the core density ρ_{core} for two ocean salinity values of 0 & 5 wt%, using two ocean temperatures T_b 255 & 270 K (Fig. 5.7 & Fig. 5.8).

ρ_{mantle} = **2500 kg m^{-3}** ρ_{core} = **5150 kg m^{-3}**					
	0 wt%			5 wt%	
T_b [K]	255	270		255	270
q_b [mW m^{-2}]	3.85	12.65		4.06	15,377
Ih-ice [km]	137.896	44.86		130.741	36.906
Liquid [km]	110.094	478.539		121.175	502.867
III-ice [km]	0	0		0	0
V-ice [km]	164.017	0		153.722	0
VI-ice [km]	245.152	117.563		268.387	150.133
R_{mantle} [km]	1976.941	1993.137		1960.075	1944.194
R_{core} [km]	1113.1	1113.911		1123.363	1141.781

Table 5.7: PhaseDiag : Structure of Ganymede for 0 and 5 wt% salt concentration and T_b={255, 270} K in the ocean, for density of the mantle ρ_{mantle} equal to 2500 kg m^{-3} and density of the core ρ_{core} equal to 5150 kg m^{-3}.

ρ_{mantle} = **2500 kg m^{-3}** ρ_{core} = **7030 kg m^{-3}**					
	0 wt%			5 wt%	
T_b [K]	255	270		255	270
q_b [mW m^{-2}]	3.85	12.65		4.06	15.38
Ih-ice [km]	137.896	44.860		130.741	36.906
Liquid [km]	110.094	478.539		121.175	502.867
III-ice [km]	0	0		0	0
V-ice [km]	164.017	0		153.722	0
VI-ice [km]	225.929	98.919		247.357	126.236
R_{mantle} [km]	1996.164	2011.781		1981.106	1968.090
R_{core} [km]	908.020	909.056		915.259	928.587

Table 5.8: PhaseDiag : Structure of Ganymede for 0 and 5 wt% salt concentration and T_b={255,270} K in the ocean, for density of the mantle ρ_{mantle} equal to 2500 kg m^{-3} and density of the core ρ_{core} equal to 7030 kg m^{-3}.

ρ_{mantle} = **2500 kg m^{-3}** ρ_{core} = **8000 kg m^{-3}**					
	0 wt%			5 wt%	
T_b [K]	255	270		255	270
q_b [mW m^{-2}]	3.85	12.65		4.06	15.38
Ih-ice [km]	137.896	44.860		130.741	36.906
Liquid [km]	110.094	478.539		121.175	502.867
III-ice [km]	0	0		0	0
V-ice [km]	164.017	0		153.722	0
VI-ice [km]	221.435	94.517		242.600	121.041
R_{mantle} [km]	2000.658	2016.184		1985.863	1973.285
R_{core} [km]	845.909	846.915		852.553	864.791

Table 5.9: PhaseDiag : Structure of Ganymede for 0 and 5 wt% salt concentration and T_b={255, 270} K in the ocean, for density of the mantle ρ_{mantle} equal to 2500 kg m^{-3} and density of the core ρ_{core} equal to 8000 kg m^{-3}.

ρ_{mantle} = **3250 kg m^{-3}** ρ_{core} = **5150 kg m^{-3}**					
	0 wt%			5 wt%	
T_b [K]	255	270		255	270
q_b [mW m^{-2}]	3.85	12.65		4.06	15.38
Ih-ice [km]	137.896	44.860		130.741	36.906
Liquid [km]	110.094	478.539		121.175	502.867
III-ice [km]	0	0		0	0
V-ice [km]	164.017	0		153.722	0
VI-ice [km]	394.939	269.567		414.598	291.954
R_{mantle} [km]	1827.154	1841.133		1813.865	1802.373
R_{core} [km]	795.646	784.880		829.756	876.159

Table 5.10: PhaseDiag : Structure of Ganymede for 0 and 5 wt% salt concentration and T_b={255, 270} K in the ocean, for density of the mantle ρ_{mantle} equal to 3250 kg m^{-3} and density of the core ρ_{core} equal to 5150 kg m^{-3}.

ρ_{mantle} = **3250 kg m^{-3}** ρ_{core} = **7030 kg m^{-3}**					
	0 wt%			5 wt%	
T_b [K]	255	270		255	270
q_b [mW m^{-2}]	3.85	12.65		4.06	15.38
Ih-ice [km]	137.896	44.860		130.741	36.906
Liquid [km]	110.094	478.539		121.175	502.867
III-ice [km]	0	0		0	0
V-ice [km]	164,017	0		153,722	0
VI-ice [km]	392.692	267.495		411.593	287.538
R_{mantle} [km]	1829.401	1843.205		1816.869	1806.789
R_{core} [km]	623.031	614.835		648.083	681.387

Table 5.11: PhaseDiag : Structure of Ganymede for 0 and 5 wt% salt concentration and T_b={255, 270} K in the ocean, for density of the mantle ρ_{mantle} equal to 3250 kg m^{-3} and density of the core ρ_{core} equal to 7030 kg m^{-3}.

ρ_{mantle} = **3250 kg m^{-3}** ρ_{core} = **8000 kg m^{-3}**					
	0 wt%			5 wt%	
T_b [K]	255	270		255	270
q_b [mW m^{-2}]	3.85	12.65		4.06	15.38
Ih-ice [km]	137.896	44.860		130.741	36.906
Liquid [km]	110.094	478.539		121.175	502.867
III-ice [km]	0	0		0	0
V-ice [km]	164.017	0		153.722	0
VI-ice [km]	392.193	266.977		410.842	286.759
R_{mantle} [km]	1829.900	23		1817.620	1807.568
R_{core} [km]	575.339	567.579		597.802	628.865

Table 5.12: PhaseDiag : Structure of Ganymede for 0 and 5 wt% salt concentration and T_b={255, 270} K in the ocean, for density of the mantle ρ_{mantle} equal to 3250 kg m^{-3} and density of the core ρ_{core} equal to 8000 kg m^{-3}.

ρ_{mantle} = **3550 kg m^{-3}** ρ_{core} = **5150 kg m^{-3}**					
	0 wt%			5 wt%	
T_b [K]	255	270		T 255	270
q_b [mW m^{-2}]	3.85	12.65		4.06	15.38
Ih-ice [km]	137.896	44.86		130.741	36.906
Liquid [km]	110.094	478.539		121.175	502.867
III-ice [km]	0	0		0	0
V-ice [km]	164.017	0		153.722	0
VI-ice [km]	442.621	317.731		460.664	336.370
R_{mantle} [km]	1779.472	1792.969		1767.798	1757.956
R_{core} [km]	445.179	392.591		553.330	655.739

Table 5.13: PhaseDiag : Structure of Ganymede for 0 and 5 wt% salt concentration and T_b={255, 270} K in the ocean, for density of the mantle ρ_{mantle} equal to 3550 kg m^{-3} and density of the core ρ_{core} equal to 5150 kg m^{-3}.

ρ_{mantle} = **3550 kg m^{-3}** ρ_{core} = **7030 kg m^{-3}**					
	0 wt%			5 wt%	
T_b [K]	255	270		255	270
q_b [mW m^{-2}]	3.85	12.65		4.06	15.38
Ih-ice [km]	137.896	44.86		130.741	36.906
Liquid [km]	110.094	478.539		121.175	502.867
III-ice [km]	0	0		0	0
V-ice [km]	164.017	0		153.722	0
VI-ice [km]	442.621	317.731		460.414	335.591
R_{mantle} [km]	1779.722	1792.969		1768.049	1758.736
R_{core} [km]	347.217	303.008		424.337	500.090

Table 5.14: PhaseDiag : Structure of Ganymede for 0 and 5 wt% salt concentration and T_b={255, 270} K in the ocean, for density of the mantle ρ_{mantle} equal to 3550 kg m^{-3} and density of the core ρ_{core} equal to 7030 kg m^{-3}.

ρ_{mantle} = **3550 kg m^{-3}** ρ_{core} = **8000 kg m^{-3}**					
	0 wt%			5 wt%	
T_b [K]	255	270		255	270
q_b [mW m^{-2}]	3.85	12.65		4.06	15.38
Ih-ice [km]	137.896	44.860		130.741	36.906
Liquid [km]	110.094	478.539		121.175	502.867
III-ice [km]	0	0		0	0
V-ice [km]	164.017	0		153.722	0
VI-ice [km]	442.621	317.731		460.417	335.331
R_{mantle} [km]	1779.722	1792.969		1768.049	1758.995
R_{core} [km]	319.895	279.165		390.947	458.858

Table 5.15: PhaseDiag : Structure of Ganymede for 0 and 5 wt% salt concentration and T_b={255, 270} K in the ocean, for density of the mantle ρ_{mantle} equal to 3550 kg m^{-3} and density of the core ρ_{core} equal to 8000 kg m^{-3}.

a) $\rho_{core} = 5150$ kg m^{-3}, T$_b = 255$ K

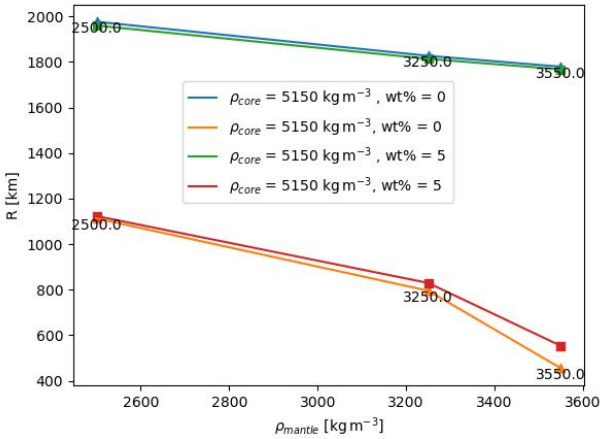

b) $\rho_{core} = 7030$ kg m^{-3}, T$_b = 255$ K

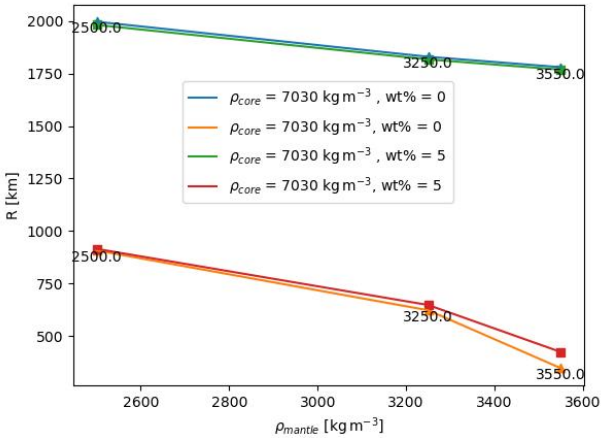

c) $\rho_{core} = 8000$ kg m^{-3}, T$_b = 255$ K

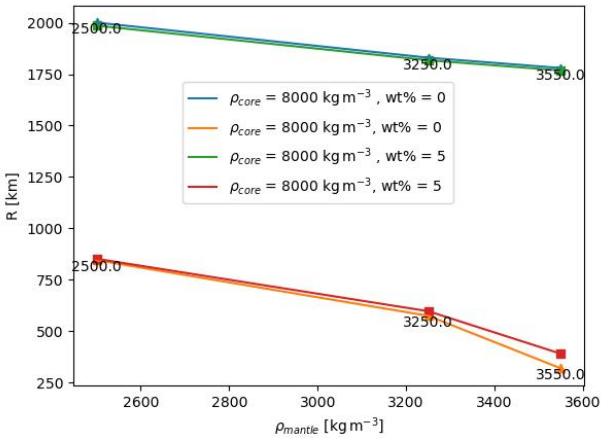

Figure 5.7: The dependence of the radius of the core R_{core} and the mantle R_{mantle} on the density of the mantle ρ_{mantle} at constant values of the density of the core ρ_{core} equal to 5150 kg m^{-3} (panel a), 7030 kg m^{-3} (panel b), and 8000 kg m^{-3} (panel c) for ocean temperature $T_b = 255$ K.

a) $\rho_{core} = 5150$ kg m^{-3}, $T_b = 270$ K

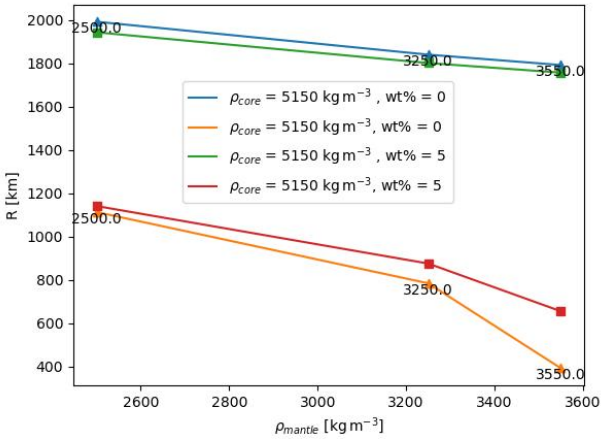

b) $\rho_{core} = 7030$ kg m^{-3}, $T_b = 270$ K

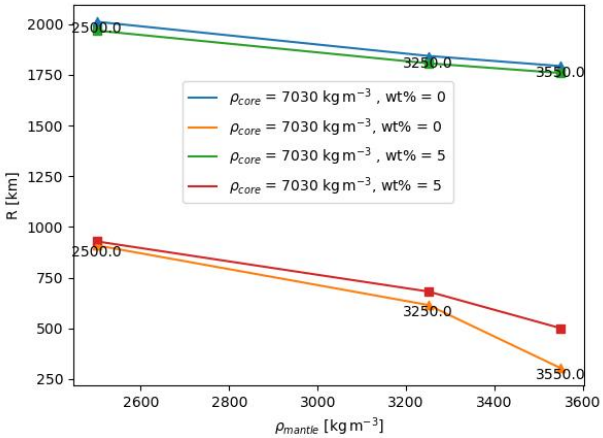

c) $\rho_{core} = 8000$ kg m^{-3}, $T_b = 270$ K

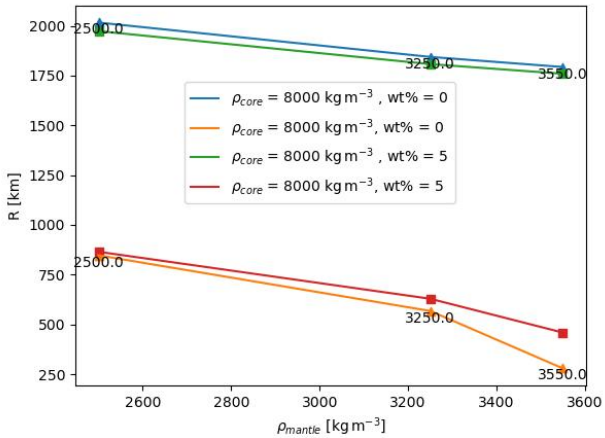

Figure 5.8: The dependence of the radius of the core R_{core} and the mantle R_{mantle} on the density of the mantle ρ_{mantle} at constant values of the density of the core ρ_{core} equal to 5150 kg m^{-3} (panel a), 7030 kg m^{-3} (panel b), and 8000 kg m^{-3} (panel c) for ocean temperature $T_b = 270$ K.

5.2 Europa

Another icy moon for which the structure was investigated was Europa, which we chose for several reasons. Current knowledge about Europa indicates a large habitability potential. Additionally, the latest findings brought by the Juno mission question the three-layer structure model for Europa. Also, in the near future, we will receive new data from Europa, specifically from the JUICE mission, which is already on its way at this time, and from the upcoming Europa Clipper mission. Since the model for Europa is unclear from the latest data, we compute the structure using two-layer and also three-layer models.

At first, we took the two-layer model. The reference parameters are listed in Tab. 5.16. We used 2 values of the moment of inertia factor: MoI = 0.3405 reported in the article (Jacobson et al., 2000) and the newer value for MoI = 0.3547 reported in (Gomez Casajus et al., 2021).

Parameter	Value
T_{surf} [K]	110
M [kg]	$4{,}8{\cdot}10^{22}$
R [km]	1560.1
MoI (Jacobson et al., 2000)	0.3405
MoI (Gomez Casajus et al., 2021)	0.3547
C [kg m^2] (Jacobson et al., 2000)	$3.98{\cdot}10^{28}$
C [kg m^2] (Gomez Casajus et al., 2021)	$4.14{\cdot}10^{28}$
g_{surf} [m s^{-2}]	1.314
$\rho_{iceI_{ref}}$ [kg m^{-3}]	920

Table 5.16: Reference parameters for Europa.

For the two-layer model, the structure was calculated for zero salt concentration, at ocean temperatures in the interval T_b=$\{260, 265, 270\}$ K, using the method described in Vance et al. (2014). The resulting thicknesses of individual layers of the hydrosphere, together with the mantle radius and core density are listed in Tab. 5.17 for the MoI determined by Jacobson et al. (2000) and for MoI of Gomez Casajus et al. (2021). The phase diagrams are shown in Fig. 5.9 for Gomez Casajus et al. (2021) and Fig. 5.10 for Jacobson et al. (2000).

By comparing the tables, it is obvious, that the ice shell thickness, and consequently, the heat flux is not much influenced by the change in MoI. We do not observe any HP ice in Europa's hydrosphere, which corresponds to the assumption. The only stable ice phase we observe in Europa's hydrosphere is Ih-ice. This means that there are no restrictions for direct contact between the ocean and silicates, which is necessary for the origin of life. In very exotic cases (specifically, for the MoI proposed by Jacobson et al. (2000), T_b=248 K and 5 wt%), the existence of III-ice with a size of around 3km was detected. In the case of MoI = 0.3405 (Jacobson et al., 2000), a higher thickness of the liquid layer was found than in the case of MoI = 0.3547 (Gomez Casajus et al., 2021) and, conversely, a smaller radius of the mantle R_{mantle}. From this, we can conclude that the thickness of the subsurface ocean decreases for higher MoI. At the same time, its thickness grows with the increasing temperature of the ocean T_b, which we also observed in the case of Ganymede.

	Europa, Gomez			Europa, Jacobson		
	N_1 = 21*50 N_2= 200*50					
T_b [K]	260	265	270	260	265	270
q_b [mW m^{-2}]	4.63	6.48	11.84	4.63	6.48	11.84
Ih-ice [km]	117.413	85.777	47.936	117.413	85.777	47.936
Liquid [km]	17.314	50.574	90.436	64.639	98.052	138,226
III-ice [km]	0	0	0	0	0	0
V-ice [km]	0	0	0	0	0	0
VI-ice [km]	0	0	0	0	0	0
R_{mantle} [km]	1425.373	1423.749	1421.728	1378.049	1376.271	1373.939
R_{core} [km]	0	0	0	0	0	0
ρ_{core} [kg m^{-3}]	3661.034	3661.861	3663.827	3935.651	3937.826	3942.321

Table 5.17: PhaseDiag - 0 wt%: Results for the two-layer structure of Europa using MoI from Gomez Casajus et al. (2021) and MoI from Jacobson et al. (2000).

Since the model is unclear in the case of Europa, we also calculated the structure of Europa using a three-layer model. Again, the reference values from Tab. 5.16 were used. The computation was performed for T_b=$\{265, 270\}$ K, because for lower temperature values it was not possible to find the corresponding ocean pressures P_b in the case of Europa for the given physical parameters. Values {0,3,5,10} wt% were used. The resulting thicknesses of the individual layers are listed in Tab. 5.18 - Tab. 5.21.

From the results, we can see that even in the case of Europa we are following the same trend as in Ganymede: As the concentration of salt in the ocean increases, the layer of Ih-ice shrinks and thus the thickness of the liquid layer increases. Of course, the heat flux also increases. When we compare the results based on the MoI value, we observe that MoI has no effect on the heat flux value, nor on the thickness of the Ih-ice layer. The difference is only in the case of the liquid layer, which in the case of MoI from Gomez Casajus et al. (2021) is significantly smaller than in the case of Jacobson et al. (2000). We see that for the case where T_b=265 K and 0 wt%, we have an almost non-existent subsurface ocean for Gomez's MoI. So again, a higher MoI value gives us smaller layers of liquid. As in the case of the two-layer model of Europa, there are no HP ices in any case.

PhaseDiag - 0 wt%	Europa, Gomez			Europa, Jacobson	
T_b [K]	265	270		265	270
q_b [mW m^{-2}]	6.48	11.84		6.48	11.84
Ih-ice [km]	85.777	47.936		85.777	47.936
Liquid [km]	3.539	43.252		26.983	66.996
R_{mantle} [km]	1470.785	1468.912		1447.341	1445.169
R_{core} [km]	523.377	523.517		612.917	613.766

Table 5.18: PhaseDiag- 0 wt%: Results for the three-layer structure of Europa using MoI from Gomez Casajus et al. (2021) and MoI from Jacobson et al. (2000).

PhaseDiag - 3 wt%	Europa, Gomez			Europa, Jacobson	
T_b [K]	265	270		265	270
q_b [mW m^{-2}]	6.82	13.09		6.82	13.09
Ih-ice [km]	81.526	43.357		81.526	43.357
Liquid [km]	8.133	48.844		31.940	72.963
R_{mantle} [km]	1470.441	1467.899		1446.634	1443.781
R_{core} [km]	523.460	524.072		612.997	614.067

Table 5.19: PhaseDiag- 3 wt%: Results for the three-layer structure of Europa using MoI from Gomez Casajus et al. (2021) and MoI from Jacobson et al. (2000).

PhaseDiag - 5 wt%	Europa, Gomez			Europa, Jacobson	
T_b [K]	265	270		265	270
q_b [mW m^{-2}]	7.15	14.36		7.15	14.36
Ih-ice [km]	77.706	39.522		77.706	39.522
Liquid [km]	12.305	53.378		36.471	77.861
R_{mantle} [km]	1470.089	1467.200		1445.924	1442.716
R_{core} [km]	523.417	523.800		613.333	614.192

Table 5.20: PhaseDiag- 5 wt%: Results for the three-layer structure of Europa using MoI from Gomez Casajus et al. (2021) and MoI from Jacobson et al. (2000).

PhaseDiag - 10 wt%	Europa, Gomez			Europa, Jacobson	
T_b [K]	265	270		265	270
q_b [mW m^{-2}]	8.58	20.68		8.58	20.68
Ih-ice [km]	64.756	27.445		64.756	27.445
Liquid [km]	26.919	68.363		51.744	93.655
R_{mantle} [km]	1468.425	1464.292		1443.600	1439.003
R_{core} [km]	523.586	525.012		613.389	615.258

Table 5.21: PhaseDiag- 10 wt%: Results for the three-layer structure of Europa using MoI from Gomez Casajus et al. (2021) and MoI from Jacobson et al. (2000).

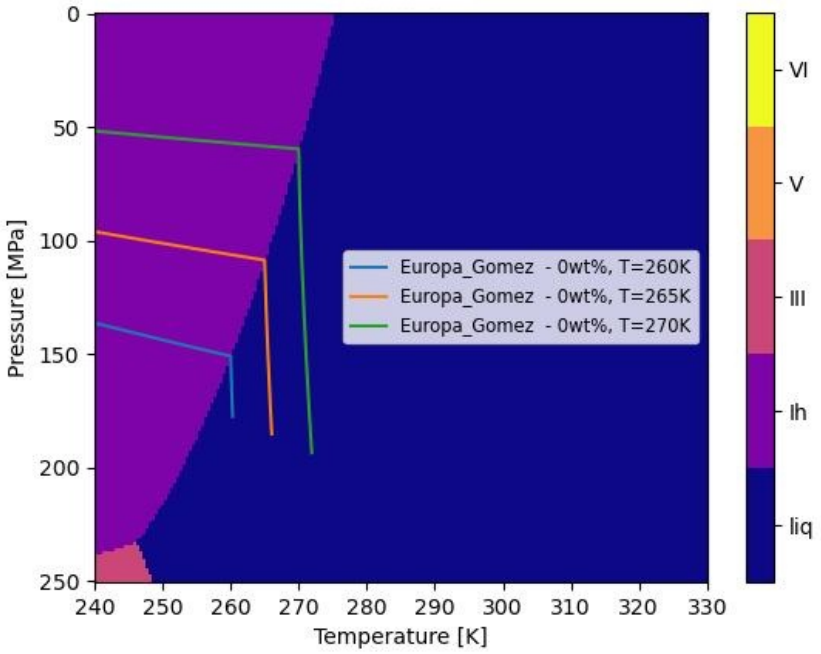

Figure 5.9: Phase diagram and temperature profile for Europa for the two-layer model, using MoI proposed Gomez Casajus et al. (2021), with 0 wt% salt concentration in the ocean, using PhaseDiag method.

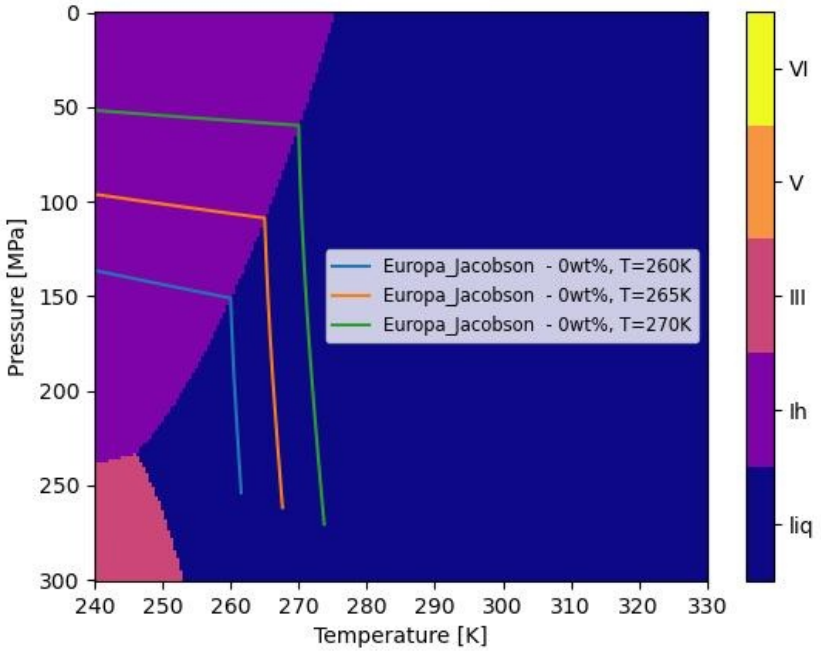

Figure 5.10: Phase diagram and temperature profile for Europa for the two-layer model, using MoI proposed by Jacobson et al. (2000), with 0 wt% salt concentration in the ocean, using PhaseDiag method.

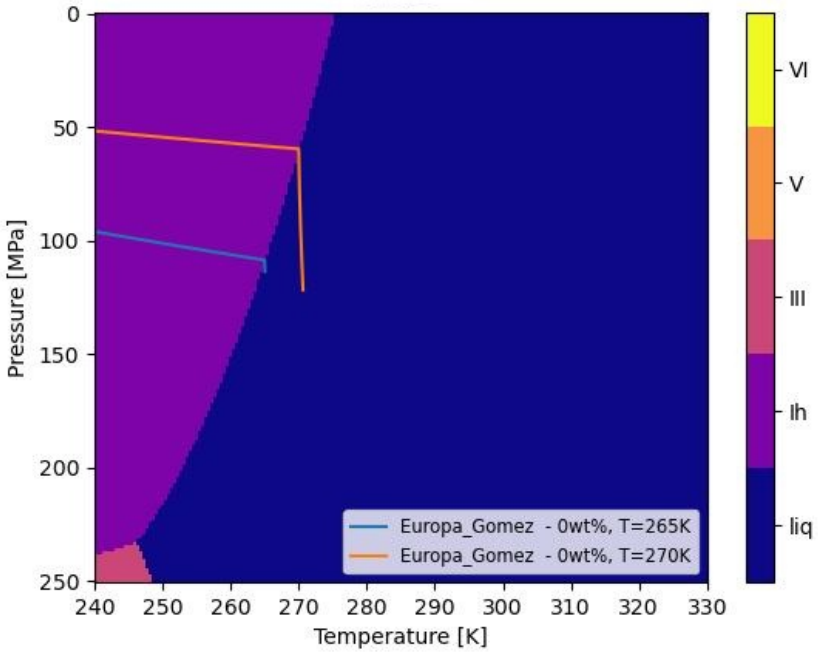

Figure 5.11: Phase diagram and temperature profile for Europa for the three-layer model, using MoI proposed by Gomez Casajus et al. (2021), with 0 wt% salt concentration in the ocean, using PhaseDiag method.

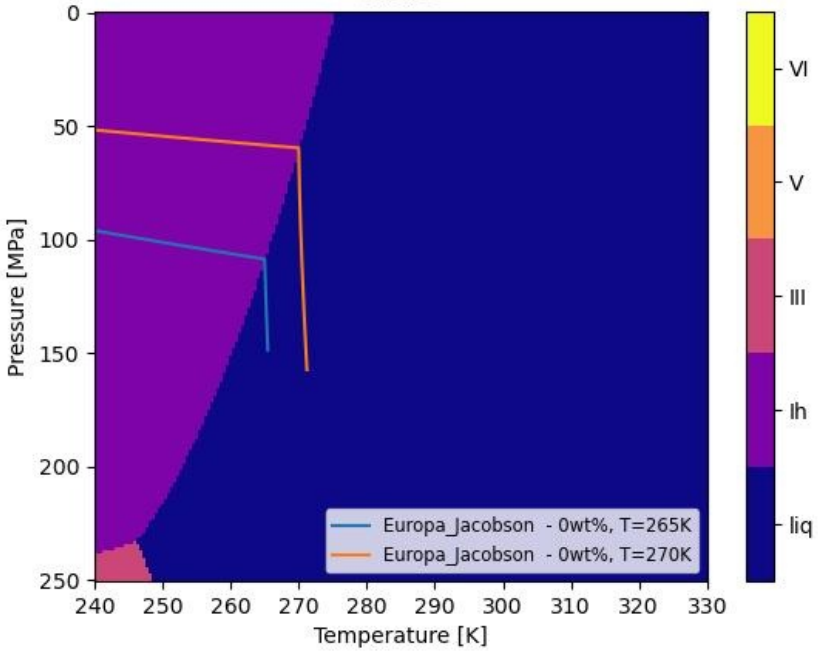

Figure 5.12: Phase diagram and temperature profile for Europa for the three-layer model, using MoI proposed by Jacobson et al. (2000), with 0 wt% salt concentration in the ocean, using PhaseDiag method.

Conclusion

An algorithm was created to determine the structure of two icy moons, namely Ganymede and Europa, using thermodynamic relations and known satellite properties, namely radius, mass and moment of inertia. Two procedures were used to calculate thermodynamic parameters. The first used the method proposed by Choukroun and Grasset (2010) and Vance et al. (2014), the second used the open-source SeaFreeze library, which we used for Ganymede. The internal structure was determined for ocean temperature between 255K and 270K and for concentrations of magnesium sulfate {0,3,5,10} wt% in the subsurface ocean.

For Ganymede, it was found that a subsurface ocean exists in the hydrosphere and that its thickness can reach up to 700 km for a salt concentration of 10 wt%. In Ganymede's hydrosphere, there are also present stable high-pressure phases of ice even at ocean salt concentrations of 10 wt%. They can thus prevent direct contact and the transfer of nutrients between silicates and the ocean. The probability of the origin of life on Ganymede is, therefore, small.

For Europa, a structure was determined for two MoI values, the value taken from the article Jacobson et al. (2000) and the one from Gomez Casajus et al. (2021), which already includes additional data from the Juno mission. Since the latest data point to the fact that Europa does not need to have differentiated deeper interior into mantle and core, a model for three different material layers, as well as a model for two different material layers, was used.

We found that the presence of high-pressure phase ice in Europa's hydrosphere is very unlikely, except in very exotic cases. Thus, direct contact between the ocean and the silicates is not prevented. However, it was also found that when using the newer MoI value and taking the three-layer material model, the thickness of the ocean layer is thin, with the highest value reaching only about 26 km for a salinity of 10 wt%. For zero concentration, the thickness was as low as 3 km. Such a thin ocean and hydrosphere could present a major obstacle to Europa's habitability.

It should be noted that in our work, a simplified structure was used for the deeper parts of the satellites. Thus, the work could be further extended in the future by including a more realistic description of silicates and iron. Similarly, the temperature profile corresponding to the convection heat transfer in the Ih-ice layer can be taken into account. Additionally, a statistical analysis could be incorporated to provide a more comprehensive understanding of icy moons' structure.

Bibliography

Andersson, Ove and Akira Inaba (2005). "Thermal conductivity of crystalline and amorphous ices and its implications on amorphization and glassy water". In: *Phys. Chem. Chem. Phys.* 7 (7), pp. 1441–1449. DOI: 10.1039/B500373C.

Bierson, Carver J. and Francis Nimmo (2022). "A note on the possibility of subsurface oceans on the uranian satellites". In: *Icarus* 373, p. 114776. DOI: https://doi.org/10.1016/j.icarus.2021.114776.

Bollengier, Olivier, J. Michael Brown, and George H. Shaw (2019). "Thermodynamics of pure liquid water: Sound speed measurements to 700 MPa down to the freezing point, and an equation of state to 2300 MPa from 240 to 500 K". In: *The Journal of Chemical Physics* 151.5, p. 054501. DOI: 10.1063/1.5097179.

Callen, H.B. (1985). *Thermodynamics and an introduction to thermostatistics, 2nd ed.* Wiley, New York.

Castillo-Rogez, Julie et al. (2023). "Compositions and Interior Structures of the Large Moons of Uranus and Implications for Future Spacecraft Observations". In: *Journal of Geophysical Research: Planets* 128.1. e2022JE007432 2022JE007432, e2022JE007432. DOI: https://doi.org/10.1029/2022JE007432.

Choukroun, Mathieu and O. Grasset (2007). "Thermodynamic model for water and high-pressure ices up to 2.2 GPa and down to the metastable domain". In: *The Journal of chemical physics* 127, p. 124506. DOI: 10.1063/1.2768957.

Choukroun, Mathieu and O. Grasset (2010). "Thermodynamic data and modeling of the water and ammonia-water phase diagrams up to 2.2 GPa for planetary geophysics". In: *The Journal of chemical physics* 133, p. 144502. DOI: 10.1063/1.3487520.

Engel, Edgar, Andrea Anelli, Michele Ceriotti, Chris Pickard, and Richard Needs (2018). "Mapping uncharted territory in ice from zeolite networks to ice structures". In: *Nature Communications* 9. DOI: 10.1038/s41467-018-04618-6.

Gomez Casajus, Luis et al. (2021). "Updated Europa gravity field and interior structure from a reanalysis of Galileo tracking data". In: *Icarus* 358, 114187. DOI: 10.1016/j.icarus.2020.114187.

Howell, Samuel M. (2021). "The Likely Thickness of Europa's Icy Shell". In: *The Planetary Science Journal* 2.4, p. 129. DOI: 10.3847/PSJ/abfe10.

Hussmann, H. et al. (2010). "Implications of Rotation, Orbital States, Energy Sources, and Heat Transport for Internal Processes in Icy Satellites". In: *Space Science Rev.* 153, pp. 317–348. DOI: 10.1007/s11214-010-9636-0.

Jacobson, R.A., R.J. Haw, T.P. McElrath, and P. Antreasian (2000). "A comprehensive orbit reconstruction for the Galileo prime mission in the J2000 system". In: *Advances in the Astronautical Sciences* 103, pp. 465–476.

Journaux, Baptiste et al. (2020a). "Holistic Approach for Studying Planetary Hydrospheres: Gibbs Representation of Ices Thermodynamics, Elasticity, and the Water Phase Diagram to 2,300 MPa". In: *Journal of Geophysical Research: Planets* 125. DOI: 10.1029/2019JE006176.

Journaux, Baptiste et al. (2020b). "Large Ocean Worlds with High-Pressure Ices". In: *Space Science Reviews* 216. DOI: 10.1007/s11214-019-0633-7.

Kalousová, K., C. Sotin, G. Tobie, G. Choblet, and O. Grasset (2018). "Two-phase convection in Ganymede's high-pressure ice layer - Implications for its geological evolution". In: *Icarus* 299, pp. 133–147. DOI: 10.1016/j.icarus.2017.07.018.

Khurana, K.K. et al. (1998). "Induced magnetic fields as evidence for subsurface oceans in Europa and Callisto". In: *Nature* 395, pp. 777–780.

Kivelson, M. G., K. K. Khurana, and M. Volwerk (2002). "The Permanent and Inductive Magnetic Moments of Ganymede". In: *Icarus* 157, pp. 507–522. DOI: 10.1006/icar.2002.6834.

Komatsu, Kazuki (2022). "Neutrons meet ice polymorphs". In: *Crystallography Reviews* 28.4, pp. 224–297. DOI: 10.1080/0889311X.2022.2127148.

Košíková, Terézia (2022). *Stabilita vysokotlakových fázy ľadu v ľadových mesiacoch*. GitLab source. SFG Student Faculty Grant, Faculty of Mathematics and Physics.

Košíková, Terézia (2023). *The structure of icy satellites*. https://gitlab.com/Terezia_Kosikova/the-structure-of-icy-satellites.git. Code for Bachelor Thesis, Faculty of Mathematics and Physics.

Lewis, John S. (1971). "Satellites of the outer planets: Their physical and chemical nature". In: *Icarus* 15.2, pp. 174–185. DOI: https://doi.org/10.1016/0019-1035(71)90072-8.

Lissauer, J.J and I. de Pater (2013). *Fundamental planetary science: physics, chemistry and habitability*. Cambridge University Press.

McNaught, A. D. and A. Wilkinson (1997). *Compendium of Chemical Terminology, 2nd ed. (the "Gold Book")*. Blackwell Scientific Publications.

Nimmo, Francis (2018). "Icy Satellites: Interior Structure, Dynamics, and Evolution". In: *Oxford Research Encyclopedia of Planetary Science*.

Reynard, Bruno and Christophe Sotin (2023). "Carbon-rich icy moons and dwarf planets". In: *Earth and Planetary Science Letters* 612, p. 118172. DOI: https://doi.org/10.1016/j.epsl.2023.118172.

Schubert, Gerald, J. D. Anderson, Tilman Spohn, and William B. McKinnon (2004). "Interior composition, structure and dynamics of the Galilean satellites". In.

Schubert, Gerald, Keke Zhang, Margaret G. Kivelson, and John D. Anderson (1996). "The magnetic field and internal structure of Ganymede". In: 384.6609, pp. 544–545. DOI: 10.1038/384544a0.

Sohl, F, T Spohn, D Breuer, and K Nagel (2002). "Implications from Galileo observations on the interior structure and chemistry of the Galilean satellites". In: *Icarus* 157.1, pp. 104–119. DOI: 10.1006/icar.2002.6828.

Šrámek, Ondřej, Yanick Ricard, and David Bercovici (2007). "Simultaneous melting and compaction in deformable two-phase media". In: *Geophysical Journal International* 168.3, pp. 964–982. DOI: 10.1111/j.1365-246X.2006.03269.x.

Taubner, Ruth-Sophie et al. (2020). "Experimental and Simulation Efforts in the Astrobiological Exploration of Exooceans". In: 216.1, 9, p. 9. DOI: 10.1007/s11214-020-0635-5.

Valencia, D., R. J. O'Connell, and D. Sasselov (2006). "Internal structure of massive terrestrial planets". In: *Icarus* 181.2, pp. 545–554. DOI: 10.1016/j.icarus.2005.11.021.

Vance, S D, K P Hand, and R T Pappalardo (2016). "Geophysical controls of chemical disequilibria in Europa". In: *Geophys. Res. Let.* 43.10, pp. 4871–4879. DOI: 10.1002/2016GL068547.

Vance, S., M. Bouffard, M. Choukroun, and C. Sotin (2014). "Ganymede's internal structure including thermodynamics of magnesium sulfate oceans in contact with ice". In: *Plan. Space Sci.* 96, pp. 62–70. DOI: 10.1016/j.pss.2014.03.011.

Vance, S. and J. M. Brown (2013). "Thermodynamic properties of aqueous $MgSO_4$ to 800 MPa at temperatures from −20 to 100°C and concentrations to 2.5 mol kg^{-1} from sound speeds, with applications to icy world oceans". In: *Geochim. Cosmochim. Acta* 110, pp. 176–189. DOI: 10.1016/j.gca.2013.01.040.

Weissman, Paul, Lucy Mcfadden, and Torrence Johnson (2007). "The Encyclopedia of the Solar System". In: *AAS/Division for Extreme Solar Systems Abstracts*.

Wikipedia (2023). *Wikipedia: Phase Diagram*. https://en.wikipedia.org/wiki/Phase_diagram. Online; accessed 15 July 2023.

List of Figures

List of Tables

List of Abbreviations

HP High-pressure

MoI Moment of inertia factor